THE LINK BETWEEN CONVECTION AND CRYSTALLIZATION IN A SUB-AXIAL MAGMA CHAMBER AND HEAT OUTPUT IN A SEAFLOOR HYDROTHERMAL SYSTEM

A Thesis
Presented to
The Academic Faculty

By

Lei Liu

In Partial Fulfillment
Of the Requirements for the Degree
Master of Science in the
School of Earth and Atmospheric Sciences

Georgia Institute of Technology

August, 2007

THE LINK BETWEEN CONVECTION AND CRYSTALLIZATION IN A SUB-AXIAL MAGMA CHAMBER AND HEAT OUTPUT IN A SEAFLOOR HYDROTHERMAL SYSTEM

Approved by:

Dr. Robert Lowell, Advisor
School of Earth and Atmospheric Sciences
Georgia Institute of Technology

Dr. Leonid Germanovich
School of Civil and Environmental Engineering
Georgia Institute of Technology

Dr. Andrew Newman
School of Earth and Atmospheric Sciences
Georgia Institute of Technology

Date Approved: July 9, 2007

ACKNOWLEDGEMENTS

I would like to particularly thank my advisor, Dr. Robert Lowell who has not only advised and directed my research; he has also shown me the joy and fun of accomplishing basic science research. I would also thank Dr. Leonid Germanovich and Dr. Andrew Newman for their guidance and helpful revisions during the course of the writing of this thesis. Research was supported by the National Science Foundation grants OCE-0527208 to Dr. Robert Lowell and Dr. Leonid Germanovich.

During the two years of my study, I have received a helping hand from many of my friends and colleagues in the geophysics group of EAS.

Finally, I must express my gratefulness for my family for their continued support and encouragement in my academic endeavors.

TABLE OF CONTENTS

LIST OF TABLES

LIST OF FIGURES

LIST OF SYMBOLS

Values of the physical parameters for hydrothermal vent fields

Physical meaning	Parameter	Value	Units
Horizontal magma area in chamber	A_m	variable	m^2
Area of hydrothermal discharge zone	A_d	10^3-10^4	m^2
Magma specific heat	C_p	1400	J /kg ºC
Fluid specific heat	C_f	6×10^3	J /kg ºC
Magma chamber depth	D	100	m
Magmatic heat flux	F	Eq.(4)	W/m^2
Acceleration due to gravity	g	9.81	m/s^2
Permeability	k	10^{-11}-10^{-13}	m^2
Latent heat of crystallization of magma	$L_{b,a}$	4.2×10^5	J/kg
Mass of magma	M		kg
Nusselt number	Nu	Eq.(2)	-
Rayleigh number	Ra	Eq.(1)	-
The critical Rayleigh number	Ra_c	$\sim10^3$	-
Basalt liquidus temperature	T_{bL}	1200	ºC
Basalt solidus temperature	T_{bS}	1070	ºC
Andesite liquidus temperature	T_{aL}	1100	ºC
Andesite solidus temperature	$T_{a,awS}$	970	ºC
Hydrothermal temperature	T_h	variable	ºC
Darcian velocity	u	Eq.(22)	m/s
Volume of magma	V		m^3
Thermal expansion coefficient of magma	$\alpha_{b,a}$	5×10^{-5}	$ºC^{-1}$
Thermal expansion coefficient of fluid	α_f	10^{-3}	$ºC^{-1}$
Proportionality coefficient	γ	Eq.(25)	-
Conduction boundary layer	δ	Eq.(20)	m
Thermal diffusivity	κ	8×10^{-7}	m^2/s
Thermal conductivity factor	λ	2	Wm/ ºC
Fluid kinematic viscosity	v_f	10^{-7}	m^2/s
Basalt kinematic viscosity	v_b	10^{-1}	m^2/s
Dry andesite kinematic viscosity	v_a	15×10^{-1}	m^2/s
3 wt% andesite kinematic viscosity	v_{aw}	3×10^{-1}	m^2/s
Magma replenishment rate factor	ξ	1-10	-

(Continued)

Dry andesite density	ρ_a	2.5×10^3	kg/m^3
3 wt % H_2O andesite density	ρ_{aw}	2.4×10^3	kg/m^3
Basaltic magma density	ρ_b	2.7×10^3	kg/m^3
Fluid density	ρ_f	10^3	kg/m^3
Gabbro density	ρ_S	2.9×10^3	kg/m^3
Volume fraction of crystals	χ	Eq.(10)(11)	-

Notes: Subscripts '*b*', '*a*' and '*aw*' refer to basaltic magma, dry andesitic magma and 3wt% H_2O andesitic magma respectively; 'f' refers to fluid; 'h' refers to hydrothermal system; 'L' and 'S' refer to liquidus and solidus temperature. Thus, for example, T_{bL} is the temperature of the basaltic magma at liquidus stage.

SUMMARY

Models of high-temperature seafloor hydrothermal systems require that heat is transferred from an underlying magma body across a conducting boundary layer to the hydrothermal system. Because magma is typically at or near its liquidus, heat transfer will result in crystallization and cooling of the magma itself. In previous models of magma cooling and solidification, solidification was assumed to occur from the top downwards. Consequently, the conducting thermal boundary layer between the hydrothermal system and magma body rapidly thickened, resulting in a rapid decay in hydrothermal heat output and vents temperature.

In this thesis, I present a simple time-dependent model of heat transfer between a turbulently convecting and crystallizing magma body and the overlying hydrothermal circulation. Most of the known seafloor hydrothermal sites on faster-spreading ridges are dominated by basalt. The hydrothermal fields within parts of the Lau Basin in the Southwest Pacific are driven by andesite. To determine the different characteristics of magma-driven hydrothermal systems, two types of magma materials, basaltic and andesitic magma are considered. Two different crystallization scenarios are considered—crystals in suspension and crystals settling. In either case, I assume that large-scale convection within the magma chamber is homogenous. Also, the effect of crystallinity and water content-dependent magmatic viscosity is considered.

Based on the proposed models, the total heat output from the upper surface of

the magma chamber and the temperature in hydrothermal system are derived. The simulation results show that without magma replenishment, the heat output and hydrothermal temperature decay rapidly within about ten years. For two different crystallization distribution cases, such rapid decay is not consistent with observations.

The conflict between the simulation results and the field observations motivates the development of more accurate magma convection models. Different from the existing modeling methods, I propose to model the magma convection with replenishment. The replenishment model can be classified into two categories in terms of status of magma chamber size. To replenish the magma system without changing the magma chamber size, the heat flux decaying rate is slowed down and hydrothermal system lifetime is extended for a little longer. Although this model is more accurate than existing ones in terms of slow decaying rate of heat flux, it does not achieve a steady state as that is observed. This leads us to model replenishment with variant magma chamber size. I model the replenishment rate to be a constant and exponential decay, respectively. Thus, I assume that the magma chamber size is time-varying. Simulation results show that magma heat flux approaches a steady state over a time scale of decades. This result is consistent with the observations, which indicates the effectiveness of proposed modeling methods.

CHAPTER 1

INTRODUCTION

Seafloor hydrothermal systems play a significant role in the transport of energy between the solid Earth and the ocean floor. Circulation of seawater through the oceanic crust along the mid-ocean ridge is the principal process responsible for the formation of submarine hydrothermal systems by which heat flux is transferred from seafloor to the ocean. Nearly 25% of Earth's global heat flux, and approximately 33% of the heat flux through the ocean floor, is transferred by hydrothermal advection [*Williams and Von Herzen,* 1974; *Stein and Stein*, 1994].

In 1977, the first active fields of hot springs were discovered at the Galapagos Spreading Center [*Corliss et al.*, 1979]. The discovery of vent sites discharging fluids is the best evidence of hot hydrothermal activity at ridge crests. In 1979, the first high temperature (~380 °C) sulfide-laden black smokers at 21ºN site on the East Pacific Rise (EPR) were discovered [*Spiess et al*., 1980]. Since that time, about 280 sites of hydrothermal activities have been discovered and explored on the ocean floor [*Baker*, 2004]. The most spectacular manifestations of seafloor hydrothermal circulation are the high-temperature "black smokers "(250 °C ~ 400 °C), and the "smoke" consists of tiny metallic sulfide particles that precipitate out of hot vent fluid as it mixes with the cold oxygen seawater near 2 °C [*Tivey and Delaney*, 1986]. Buoyant plumes from such vents can be traced in the ocean for hundreds of meters upwards and hundreds of kilometers horizontally [*Baker et al*. 1995].

The style of hydrothermal venting varies with the spreading rate. On the slow-spreading Mid-Atlantic Ridge, for example, the Transatlantic Geotraverse (TAG) hydrothermal field has black smokers on the top of a large single large deposit 200 m in diameter and about 50 m in height [*Becker et al.*, 1996]. TAG hydrothermal activity is driven by periods of rapid magma supply and has been episodic over relatively long periods (10^5 years) [*Rona*, 1984; 1995]. On the intermediate-spreading Juan de Fuca Ridge, the most common structures are the large multi-flanged irregular sulfide mounds (up to 18-20 m tall) that host multiple vigorously venting black smoker chimneys on their summits [*Tivey and Delaney*, 1986; *Delaney et al.*, 1997]. On the fast-spreading East Pacific Rise, black smokers typically occur through discrete individual chimneys and chimney clusters. The sulfide chimney is rarely more than 15 m tall [*Kelley et al.*, 2002].

Studies from a number of hydrothermal sites show that the total heat output from high-temperature hydrothermal systems at oceanic spreading centers typically ranges between 10^8 and 10^9 Watts [*Lowell and Germanovich*, 2004; *Ramondenc et al.*, 2006]. These values usually come from water column measurements of integrated heat flux. The high-temperature component measured at individual vents is around 10^7 Watts. Observed heat output and vent temperature data are summarized in Table 1 (see corresponding reference for details).

Table 1.1 Vent flow characteristics for some seafloor hydrothermal systems

Reference	Location	Vent temperature (°C)	Vent Heat Flux (MW)	Integrated Heat Flux H_t (GW)
Rona and Trivett [1992]	Axial Volcano (JdFR)	108 - 326	2.4 - 6.4	
Rosenberg et al. [1988]	Endeavour (JdFR)	up to 400		1 - 5
Schultz et al. [1992]	Endeavour (JdFR)	7 - 13	53.5 – 62.9	
Veirs et al. [2006]	Endeavour (JdFR)		8 - 42	
Ginster et al. [1994]	Endeavour (JdFR)	296 - 374	3.6 - 87.3	0.29 - 0.44
Baker and Massoth [1986]	South Cleft (JdFR)			0.29 - 0.87
Baker and Massoth [1987]	Endeavour (JdFR)			0.6 - 2.8
Baker et al. [1993]	North Cleft (JdFR)	104 - 324	161 - 319	0.48 - 0.96
Baker [1994]	North Cleft (JdFR)			0.38 - 0.94
Gendron et al. [1994]	North Cleft (JdFR)			1.4 - 4
Stein and Fisher [*2001*]	Middle Valley (JdFR)	180 - 276	0.13	
Lonsdale and Becker [1985]	Southern Trough (GB)	270 - 314	86 - 201	
Ramondenc et al. [2006]	9°50′ N (EPR)	345 - 388	40	
McConachy et al. [1986]	11°N (EPR)	347	3.0 - 25	
Macdonald et al. [1980]	21°N (EPR)	344 - 356	0.2 - 0.3	
Converse et al. [1984]	21°N (EPR)	275 - 350	140 - 300	
Rudnicki and Elderfield [1992]	TAG (MAR)	360 - 364		0.5 - 0.9
Rona et al. [1993]	TAG (MAR)	365	200 - 250	
Rudnicki and German [2002]	Kairei (CIR)	360		0.07 - 0.12

Notes: In this table, JdFR stands for Juan de Fuca Ridge, GB for Guaymas Basin, EPR for East Pacific Rise, MAR for Mid-Atlantic Ridge and CIR for Central Indian Ridge. Modified from [*Lowell et al.*, 2007].

High-temperature hydrothermal circulation is often associated with differences in subsurface magma supply [e.g. *Macdonald et al.*, 1984; *Macdonald et al.*, 1992]. Seismic reflections from magma chambers have been observed along the fast-spreading ridges, such as East Pacific Rise [*Detrick et al.*, 1987; *Kent et al*., 1990, S*ingh et al.*, 1999] and the intermediate-spreading Valu Fa Ridge [*Collier and Sinha*, 1990; *Sinha* 1995; *Turner et al.*, 1999]. Sub-axial reflections also exist beneath the intermediate-spreading Juan de Fuca Ridge (JDFR) [*Rohr et al*., 1988; *Canales et al.*, 2005; *Canales et al.*, 2006] and the slow-spreading Mid-Atlantic Ridge (MAR) [*Calvert*, 1995; *Sinha et al.*, 1998; *Singh et al.*, 2006]. Moreover, observations from the 21°N sites on EPR have indicated that the considerable stability of hydrothermal venting last for more than two decades [*Campbell et al.*, 1988; *Von Damm et al.*, 2002]. The steady state character of seafloor hydrothermal systems has been linked to magma replenishment [*Lowell and Germanovich*, 1994; *Humphris and Cann*, 2000]. They argue that magma replenishment at rates similar to those observed at basaltic volcanoes could sustain hydrothermal output on decade long time scales.

A new hydrothermal field, Lost City, was discovered in December 2000, which represents the first observation of the low-temperature venting (40 °C~75 °C) [*Von Damm*, 2001]. It is distinctly different from all other known sea floor hydrothermal fields. It is located about 15 km away from a mid-oceanic ridge and on 1.5 million years old ocean crust. Seafloor hydrothermal fluids derived from serpentinization reactions, rather than by the heat of magma [*Kelley et al.*, 2001]. Lost City is characterized by massive white structures, up to 60 m high, rather than sulfide

structures typical of black smokers. This is the first major occurrence of active carbonate chimneys at a vent site [*Kelley et al.*, 2001].

The discovery of seafloor hydrothermal systems more than three decades ago has revolutionized our understanding of biological processes [*Jannasch*, 1995; *Shank et al.*, 1998] and the Earth's thermal and geochemical budgets [*Edmond et al.*, 1979]. Given the global importance and diversity in the processes, a large number of mathematical models have been developed. However, relatively few of these models have addressed the link between the high-temperature hydrothermal system and magma supply or provide a basis for understanding heat transport from a convecting magma chamber to the overlaying hydrothermal system. The objective of this work is to find out how a magma chamber can maintain a high-temperature venting steady state for decades.

The thesis is organized as following. In chapter 2, I will discuss the existing models in the literature for the seafloor hydrothermal process, magma chamber convection systems, and the interaction between them. Chapter 3 presents the fundamental theory for magma convection and hydrothermal circulation. Moreover, the comparison between basaltic and andesitic magma is discussed. The numerical simulation results of a magma convection system without replenishment model are given in Chapter 4, which demonstrates the inconsistency between theoretical models and on-site observations. In Chapter 5, I develop theoretical models of magma convection with replenishment and present the relevant simulation results and discussion. Chapter 6 includes the conclusion and suggestions for further work.

CHAPTER 2

A REVIEW OF THERMAL CONVECTION MODELS

2.1 Models of hydrothermal convection

Even before the discovery of submarine hydrothermal venting, a comparison of conductive heat flow data with models of global heat loss from cooling, spreading lithosphere suggested that hydrothermal heat loss was an important component of Earth's energy budget (Figure 2.1). *Stein and Stein* [1994] compare theoretical and observed heat flow data to parameterize hydrothermal circulation and find that the advected heat flux caused by hydrothermal circulation is significant. About 33% of the total oceanic heat flux occurs by advection and approximately 30% of the advected portion of the flux occurs in younger crust than 1 Ma. Early models of single-pass tried to explain the low conductive heat flow values measured on young crust and in terms of hydrothermal heat loss [*Bodvarsson and Lowell*, 1972; *Lowell*, 1975], whereas early models of cellular convection attempted to explain heat flow anomaly patterns observed in young sedimented lithosphere [*Williams et al.*, 1974; *Ribando et al.*, 1976; *Green et al.*, 1981; *Fehn et al.*, 1983]. Once high temperature vents were discovered, however, the importance of magmatic heat became apparent [S*trens and Cann*, 1982,1986; *Lister*, 1983; *Cann et al*. 1985; *Lowell and Rona,* 1985; *Lowell and Burnell*, 1991; *Lowell and Germanovich*, 1994].

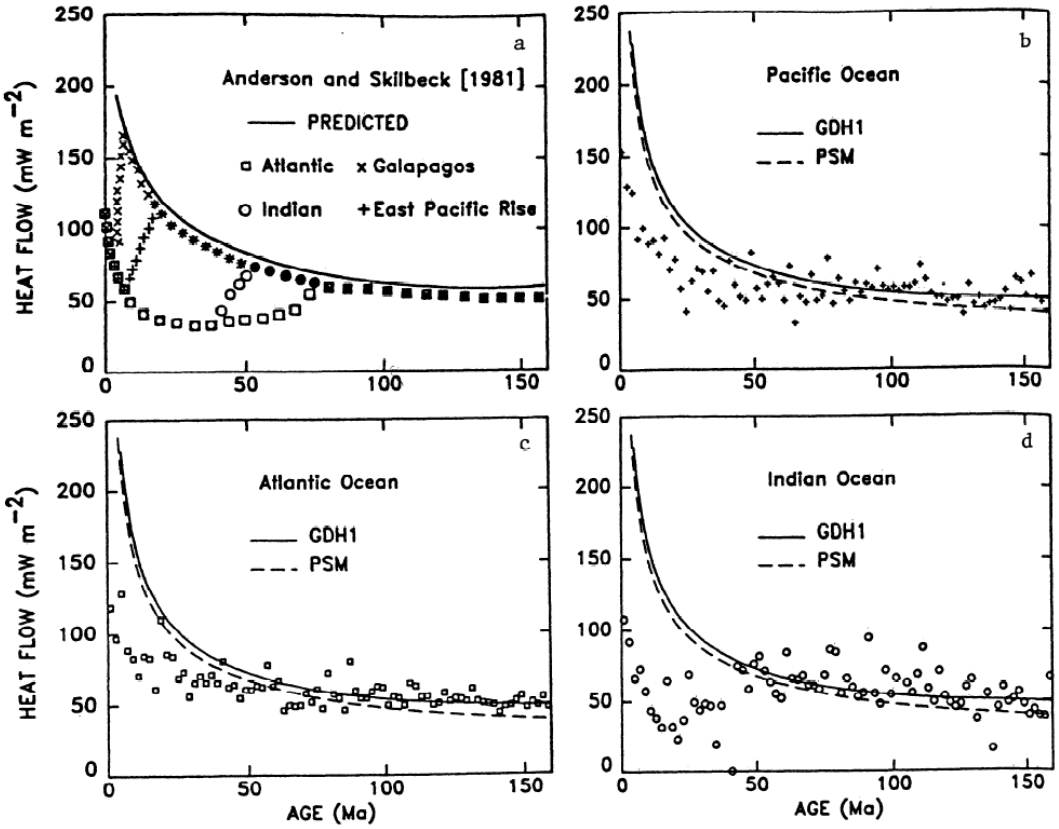

Figure 2.1: Observed and predicted heat flow versus age of the ocean basins. Figure (a) is summary of earlier results from [*Anderson and Skilbeck*, 1981, Figure 6]. The predicted curved is schematic. (b), (c) and (d) are results from *Stein and Stein* [1994] compared to predictions of reference models GDH1 [*Stein and Stein*, 1992] and PSM [*Parsons and Sclater*, 1977]. The symbols for observed heat flow are shown in (a). Similar sealing ages for all the oceans are indicated, in contrast to the earlier compilation which showed sealing at younger ages in the Pacific [From *Stein and Stein*, 1994].

In general, hydrothermal convection models can be classified into three categories: cellular convection (porous medium) models, single-pass (pipe) models and downward cracking models. Reviews of various models of hydrothermal systems can be found in *Lowell* [1991a], *Lowell et al.* [1995] and *Lowell and Germanovich* [2004].

Cellular convection models were initially developed by *Horton and Rogers*

[1945] and *Lapwood* [1948] to investigate the condition for the onset of convection in a water-saturated porous material layer. Their stability analysis served as a starting point for studying geothermal convection problems. Those papers considered a homogeneous porous layer which is heated from below. The upper and lower boundaries were considered impermeable and isothermal. For this configuration, the Rayleigh number *Ra*, a dimensionless parameter that determines onset of convection, must be greater than $4\pi^2$, although different boundary conditions yield different values of the critical Rayleigh number Ra_c [*Lapwood*, 1948]. Cellular convection models of finite amplitude ($Ra >> Ra_c$) have been applied to off-axis convection [*Lowell*, 1980; *Fisher et al.*, 1990; *Fisher and Becker*, 1995] and the ridge-axis convention (e.g., *Brikowski and Norton* [1989]; *Wilcock* [1998]; *Rabinowicz et al.* [1999]). *Schoofs and Hansen* [2000] investigated the depletion of brine layer at the base of a vigorously convecting system. *Jupp and Schultz* [2000] argued that the thermodynamic properties of water may control black smoke at 400 °C.

Single pass or pipe models examine the general behavior of the hydrothermal system without considering details of the temperature and velocity distribution. They consist of a recharge, discharge zone and heat transfer zone. These models arose initially in the study of warm springs in Iceland [e.g., *Bodvarsson*, 1950; 1961]. In the context of ocean ridge hydrothermal processes, they offer a useful conceptual model, in which cold seawater penetrates downward to an axial magma body and is heated near the interface between solidified intrusive rocks and magma. Then the fluids transfer thermal energy out of the ocean crust during rapid, buoyant rise and discharge

at the ocean floor (Figure 2.2). The pipe models can be viewed as a special case of the cellular convection models, in which an extremely heterogeneous distribution of permeability restricts the flow paths to pipe-like zones. As a result of their simplicity, pipe models have been applied to many seafloor hydrothermal problems such as conductive heat flow anomalies [*Bodvarsson and Lowell*, 1972; *Lowell,* 1975], the temporal evolution of heat transfer from solidifying magma to black smokers [*Lowell and Germanovich*, 1994], and the formation of catastrophic event plumes associated with dike injections [*Lowell and Germanovich*, 1995], and other applications of pipe models to a number of seafloor hydrothermal problems were discussed in [*Lowell and Germanovich* 2004].

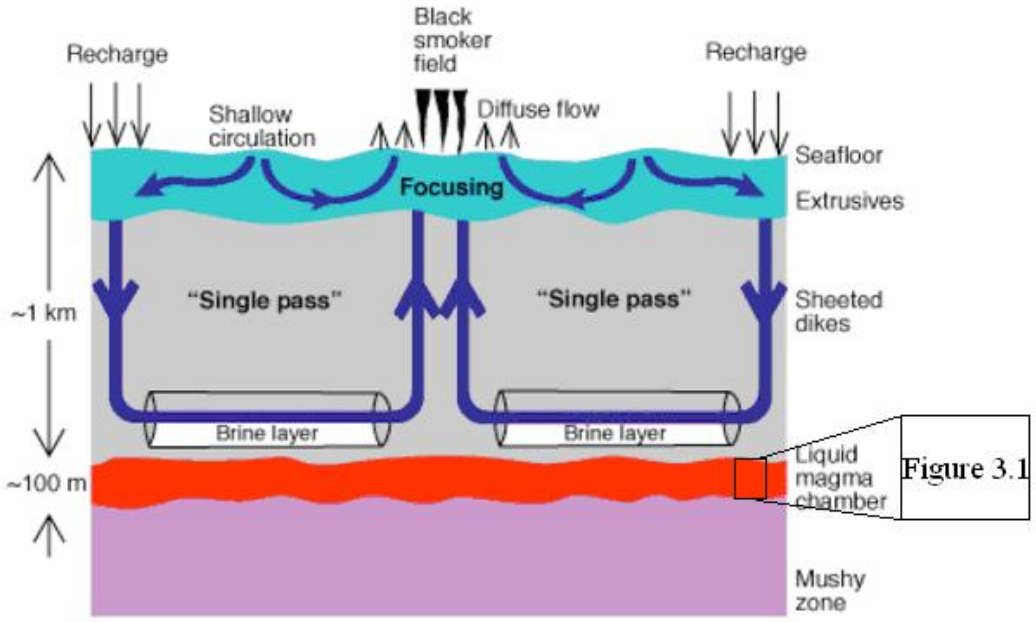

Figure 2.2: Cartoon of a single-pass hydrothermal circulation cell at a mid-ocean ridge. Here single-pass refers to the deep circulation system in which fluid circulates downward into the ocean crust, flows more or less horizontally near the top of the magma chamber at the base of the sheeted dikes, and ascends back to the surface.

Focused high-temperature flow is thought to occur in the main single-pass limb; diffuse flow may occur as a result of mixing of the deep circulation with shallower circulation in the extrusive layer, here as pillow lavas [from *Germanovich et al.,* 2000]. The diagram of a liquid magma chamber is given in Figure 3.1.

The downward cracking models were initially provided by *Lister* [1974, 1983]. He assumed that tensile thermal stresses, provided by temperature differences, could cause fracture propagation, so that hydrothermal circulation would migrate downward and extract heat from the cracked hot rock. Lister's original model is now viewed as being incorrect because it neglected the effect of rock compressive stresses as cracks propagate through the crust. *Lowell and Germanovich* [1994] suggested that thermal stresses associated with dike emplacement and cooling may be preferable to Lister's original mechanism. In consequence, as magma crystallizes the hydrothermal system migrates downwards and high heat flux is maintained. The downward cracking concept is still prevalent in the literature (e.g. [*Wilcock and Delaney*, 1996; *Kelley et al.*, 2002]).

2.2 Models of Magma Convection

It has been widely appreciated that convection plays an important dynamical role in nucleation, growth and redistribution of crystals in magma chambers. The characteristics of these processes have been investigated for different types of boundaries such as the roof, the floor and the side-wall of the magma chamber. *Huppert and Sparks* [1988] implicitly assumed that crystals grew in suspension within the interior of magma and were immediately swept away by the convection. *Worster*

et al. [1990] argued that for a small body of magma (e.g. thin sill), the crystals grew predominantly at the roof; whereas for a large magma body (hundreds of meters in height), crystallization at the floor is increasingly important, even though the cooling is only from above. *Hort* [1997] investigated a model of the solidification of magma cooling from above and found that the vigor of convection was strongly dependent on the kinetics of crystallization inside of the magma chamber. *Hort* [1997] assumed a linear relationship between magma temperature and the fraction crystallized.

Typically, there are two types of magma convections determined by the driving forces: compositional convection and thermal convection. Compositional convection results from compositional variations either because of injection of a new composition into a chamber, partial melting or fractional crystallization. The compositional variations within a chamber provide buoyancy forces that may drive convective flow. Comparatively, the convection caused by the temperature variation and heat flux out through surrounding rocks is usually called thermal convection. First models of thermal-compositional convection in magma chambers describe the mixing of incompressible homogeneous magma [*Oldenburg et al.*, 1989]. Convection is driven by compositional buoyant magma release during floor crystallization [*Jellinek and Kerr*, 1999]. Multiphase convection of crystal-bearing magma associated with vertical density gradients was considered by *Bergantz* [2000].

In this thesis, I will neglect the effects of compositional convection and use a theoretical model of magma thermal convection based on the one developed by *Huppert and Sparks* [1988] for the physics of crystallization and melting at the

chamber roof. It is helpful to introduce their model first, and to point out the key differences between their model and the one used in this thesis. According to their model, heat transfer from a vigorously convecting basaltic magma emplaced into cold continental crust results in melting in the solid chamber roof to form a silicic magma, while at the same time crystallizing and cooling occur within the basaltic magma. They assumed the crystals are suspended within the interior of the convecting magma. *Huppert and Sparks* [1988] construct a simple 0-dimensional heat balance to relate the heat loss in the vigorously convecting magma body to the heat loss through the roof of the magma chamber. To describe crystallinity as a function of time I will use both the linear relationship given by *Hort* [1997] and the reciprocal function between magma temperature and crystal content given by *Huppert and Sparks* [1988].

The first distinction between the *Huppert and Sparks* [1988] model and the model presented in the thesis lies in the upper boundary layer. My model links the heat transfer from the magma chamber to the overlying hydrothermal circulation system. Consequently, the temperature of upper boundary of the convecting magma, T_s is constant. Because hydrothermal circulation rapidly removes heat from the crustal rocks, there is no induced melting at the chamber roof. Second, the thermal conductive boundary layer between the magma chamber and overlaying hydrothermal system remains thin. However in the *Huppert and Sparks* [1988] model, the silicic magma upper boundary layer grows with time.

2.3 Linked Models of Magma and Hydrothermal Convection

The first models linking magmatic heat transfer to an overlying hydrothermal

system [e.g., *Lowell and Rona*, 1985; *Lowell and Burnell*, 1991] recognized that heat transfer from magma must result in crystallization of the magma body. These models assumed that crystallization occurred at the roof of the magma. Consequently, heat loss from the magma decreased with time and the temperature and heat output of the hydrothermal systems did also. Despite the deficiencies of these models, studies of temporal evolution in hydrothermal processes [*Haymon et al*. 1991, 1993, 1996; *Embley et al*. 1995; *Von Damm et al*. 1995; *Wright et al*. 1995], indicate that there is a close coupling between magma supply and hydrothermal processes on individual ridge segments. However, the details of the connection between ridge axis hydrothermal flux and subsurface magma chamber processes are far from clear.

It is important to point out that in studies of the hydrothermal convection at mid-ocean ridges, the boundary condition at the base of the hydrothermal system typically has two forms. In the most common situation, the temperature is fixed at the bottom, T_s. This condition assumes that magma serves as an infinite reservoir of heat. Consequently, the hydrothermal system controls how much heat is taken out. The higher the value of *Ra*, the more vigorous the convection and the greater the hydrothermal heat transport. If a constant heat flux is assumed at the base of hydrothermal system then hydrothermal heat output is controlled by the rate at which heat is conducted from the magma body. The more vigorous the convection, the cooler the temperature of the hydrothermal fluid will be. Realistically, heat transfer from a convecting mid-ocean ridge magma body will cause it to cool and crystallize. The heat reservoir is not only finite, but will decay in time. Hence the hydrothermal

circulation above a convecting magma body is expected to be time dependent.

In the following chapters, I link magma and hydrothermal models at oceanic spreading centers more realistically than in the past by including turbulent convection and crystallization of magma. I consider two scenarios of crystal distribution within a magma chamber. Similar to *Huppert and Sparks* [1988], the model assumes the convective motions in the magma chamber are sufficiently vigorous to keep crystals in suspension and well mixed within the interior of the magma. This assumption is counter to traditional models in which crystals settling can occur at the boundary layer of a magma chamber and accumulate on the floor [*Martin*, 1990; *Martin and Nokes*, 1989; *Worster et al*., 1990]. This assumption permits us to calculate an upper bound of the rate of heat transfer from the magma to the hydrothermal system because if crystals are settling during magma solidification as in some models, the thermal boundary layer would rapidly thicken [*Lowell and Germanovich* 2004]. This would result in lowering the rate of heat transport between the magma chamber and hydrothermal system. However, homogeneous crystallization of a well-mixed magma is considered only possible in the early stages of magma convection processes because of the larger density with increasing crystal content [*Brandie and Jaupart*, 1986]. Therefore, I consider another extreme case that assumes crystals instantly fall out of suspension and settle onto the chamber floor as they form within the magma. The lower boundary layer grows with time resulting in the depth of liquid magma decrease as time. This assumption allows us to calculate the maximum lifetime of the magma convection since the magma convection is driven only by the liquid magma.

CHAPTER 3

THE BASIC THEORY OF A COUPLED MAGMA-HYDROTHERMAL SYSTEM MODEL

Meaningful mathematical models must be constrained by observational data and also incorporate realistic rock and fluid physical parameters. Consequently, information on the temperature and thickness of subsurface magma bodies, along with data on the vent field provide useful modeling constraints. The density of melts ranges from 2500 kg/m^3 to 2700 kg/m^3 at magmatic temperature (~1200 °C) for basaltic magma from 2 wt% to dry at lower pressure. I select typical densities of ρ_b = 2700 kg/m^3 for basaltic, ρ_a = 2500 kg/m^3 for dry andesitic and ρ_{aw} = 2400 kg/m^3 for 3 wt% andesitic magma, respectively [*Trial and Spera*, 1990; *Spera*, 2000]. The shape and size of magma body are the most important parameters during the heat transfer. I consider a rectangular-shaped magmatic sill with planar area A_m and thickness D ($D << A_m$). The liquid magma layer D is typically several tens of meters [*Kent et al*., 1990; *MacLeod and Yaoyancq*, 2000]. In this model, D is assumed to be 100 m thick. Although the magma lens may extend for tens of kilometers along the axis at fast spreading ridges [*Sinton and Detrick*, 1992], the magma lens is 1 – 4 km in width across-axis [*Collier and Sinha*, 1990; *Kent et al.*, 1990; *Singh et al.*, 2006] and the vent field spaces 1 – 3 km along-axis [*Gente et al.*, 1986; *Kelley et al.*, 2002]. The heat uptake area A_m is thus estimated to be ~ 10^6-10^7 m^2. Magma temperature depends on the pressure. Select the typical liquidus temperature T_L for basaltic magma to be 1200 °C [*Sinton and Detrick*, 1992], and the solidus basaltic magma temperature T_{bS}

to be 1070 ºC at lower pressure. The detailed reason will be given in section 4.3. For simplification, the values of other parameters for three magma types, such as latent heat and thermal diffusivity, etc., are assumed to be the same. These experimental and field data will be used in all simulation results.

Figure 3.1 depicts a scenario of the basic model, a layer of vigorously convecting basaltic (andesitic) magma underlying a hydrothermal system with all crystals in suspension. The hydrothermal circulation system is similar to Figure 2.2, in which cold seawater penetrates into the oceanic crust where it is heated and modified to a hydrothermal fluid at a temperature T_h. Because the hydrothermal fluid is much cooler than the magma solidus temperature T_S (the temperature at the top of the magma chamber), heat is transferred from the convecting magma at temperature $T_{b,a}$ across a thermal conductive boundary layer $\delta(t)$ at a time-dependent heat flux $F_{b,a}$, where the subscripts a and b refer to andesite and basalt, respectively. Then the buoyant fluids rise rapidly, and discharge into the ocean through hydrothermal vents. As a result, the magma chamber cools down and crystallizes. As a consequence of the magma heat decay, the heat transferred to hydrothermal system is expected to decrease, resulting in the decrease of the hydrothermal temperature and heat output. Models are run until the crystallinity $\chi(T)$ of the magma chamber reaches 60%, because at which point the kinematic magma viscosity $\nu(T)$ approaches infinity [*Marsh,* 1981]. The symbols used in this thesis are all given in the LIST OF SYMBOLS beginning on page ix.

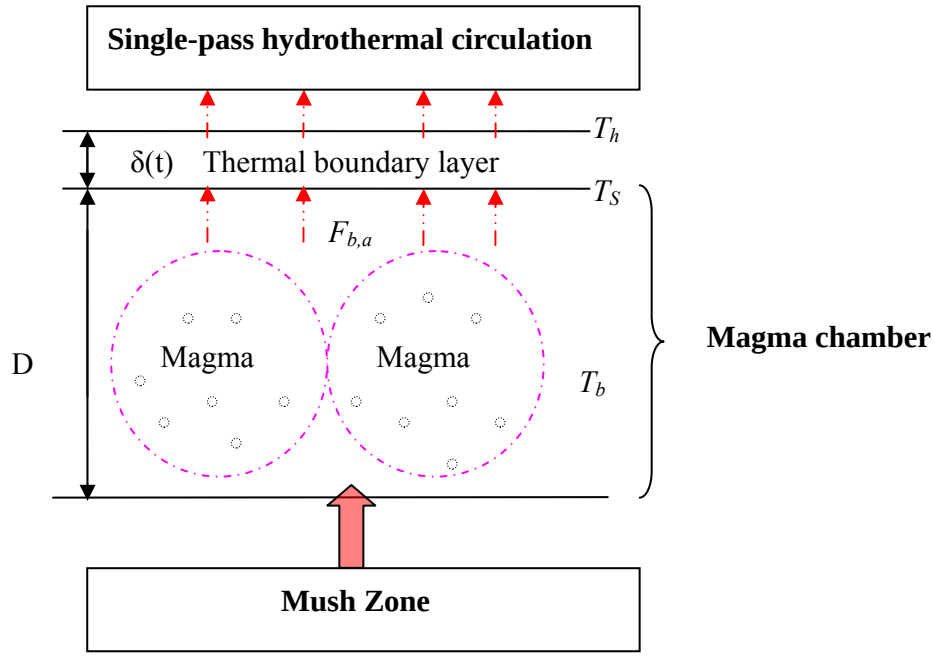

Figure 3.1: A convection magma chamber model with crystals in suspension. This is the liquid magma chamber part in Figure 2.2. The turbulent convection magma acts as a source of heat to power the overlying the hydrothermal system, at the same time the underlying mush zone provide new heat source to the magma chamber. Details of magma dynamics are neglected in this model.

In the following sections, the mathematical model is presented to describe the interactive characteristics of both the magma convection system and the hydrothermal system. Specifically, Section 3.1 develops the basic model with all crystals in suspension, but without magma replenishment; Section 3.2 describes the hydrothermal circulation; Section 3.4 develops a somewhat different model from the one in Section 3.1. Therefore, it is assumed that all crystals fall out of liquid magma and accumulate on the chamber floor. It is worth pointing out that, the proposed model in Section 3.4 does not consider the magma replenishment either.

3.1 Convection of magma system without replenishment

3.1.1 Thermal convection in magma at an oceanic spreading center

When magmas rise from the Earth's upper mantle and pond as a magma chamber, heat will be transferred by conduction between the cold county rock with temperature T_S and hot magmas with temperature $T_{b,a}$. The magmatic sill initially at its liquidus temperature T_L cooled by an overlying hydrothermal system. As shown by *Huppert and Sparks* [1988], *Martin and Nokes* [1989], *Huppert and Turner* [1990], *Worster et al.* [1990], *Jaupart and Tait* [1995] and *Jellinek and Kerr* [1999], such a magma body would undergo vigorous convection at a Rayleigh number $Ra >> Ra_c$ (the critical value).

For this system, the dimensionless parameter Ra is a measure of the strength of the convection, which is defined as the ratio of thermal buoyancy force to the viscous and thermal resistance:

$$Ra = \frac{\alpha g D^3 \Delta T(t)}{\kappa \nu (T_{b,a}(t))} \tag{1}$$

where α is the coefficient of thermal expansion, g is the acceleration due to gravity, D is the thickness of the magmatic layer, κ is the thermal diffusivity, and ν is the kinematic viscosity, respectively. The temperature difference $\Delta T(t) = T_{b,a}(t) - T_S$. The Rayleigh number is proportional to the third power of thickness of magmatic layer; hence the size of the system is the most important parameter concerning the existence

and vigor of convection. Because $\Delta T(t)$ and kinematic viscosity $\nu(T_{b,a}(t))$ are functions of time, then *Ra* is a function of time for this situation.

Following *Huppert and Sparks* [1988] we express the heat flux from the convecting magma body in terms of the Nusselt number *Nu*, which is defined as the ratio of the heat transport as a result of convection $F_{b,a}(t)$, to the heat flux conducted across the layer of thickness *D* in the absence of convection.

$$Nu = \frac{F_{b,a}(t)D}{\kappa\rho_{b,a}C_p\left(T_{b,a}(t) - T_S\right)} \tag{2}$$

where $\rho_{b,a}$ is the magma density and C_p is the specific heat of magma, respectively.

The classical relationship between the Nusselt number and the thermal Rayleigh number is given by [*Jarvis and Peltier*, 1989]:

$$Nu \approx (Ra / Ra_c)^{1/3} \tag{3}$$

Upon substituting equations (1) and (3) into equation (2), we obtain the heat flux transferred as a result of convection in the magma chamber ([*Turner*, 1973]):

$$\begin{aligned} F_{b,a}(t) &= \left(\frac{{\rho_{b,a}}^3 {C_p}^3 \alpha_{b,a} g\kappa^2 (T_{b,a}(t) - T_S)^4}{10^3 \nu_{b,a}}\right)^{1/3} \\ &= \rho_{b,a} C_p J_{b,a} (T_{b,a}(t) - T_S)^{4/3} \end{aligned} \tag{4}$$

where $J_{b,a} = 0.1(\alpha_{b,a} g\kappa^2 / \nu_{b,a})^{1/3}$.

As a result of the heat flux $F_{b,a}(t)$ transferring through the top boundary of area A_m, the magma body cools, and crystals begins to form, provided the temperature $T_{b,a}(t) < T_L$ (the liquidus temperature). In this section, we assume all the crystals are suspended interior of magma. The latent heat of crystallization is released as crystals form. The simple heat content of a mass of magma M is then given by:

$$H(t) = MC_p T_{b,a}(t) + M\left(1 - \chi\left(T_{b,a}(t)\right)\right)L_{b,a} \tag{5}$$

where $L_{b,a}$ is the latent heat of crystallization of basaltic (andesitic) magma, $\chi(T_{b,a}(t))$ is the crystal content of magma at temperature $T_{b,a}(t)$, respectively. Because the mass conservation for this case without replenishment, M is the mass of liquid-crystal mixture, $M = \rho_{b,a}V = \rho_{b,a}DA_m$, and volume of chamber V is constant. We ignore the density difference between liquid magma and crystals. The negative time derivative of the heat content is equal to the heat flow output from the magma chamber. Equation (5) can be modified by:

$$\frac{dH(t)}{dt} = -F_{b,a}(t)A_m \tag{6}$$

Combining equations (5) and (6), the heat conservation equation in the magma liquid layer across the interface is obtained [*Huppert and Sparks*, 1988]:

$$\rho_{b,a}C_p D\frac{dT_{b,a}}{dt} - \rho_{b,a}L_{b,a}D\chi'\left(T_{b,a}(t)\right)\frac{dT_{b,a}}{dt} = -F_{b,a}(t) \tag{7}$$

where $\chi'(T_{b,a})$ indicates the first order derivative of crystallinity. The calculation will be discussed in the following section. In the equation (7), the first term on the left hand side represents the rate at which temperature varies in convecting magma and the second term represents the latent heat released at the top of magma chamber, the right hand side represents the heat flux by conduction. From equation (7), the rate of magma temperature change can be expressed as:

$$\frac{dT_{b,a}}{dt} = \frac{F_{b,a}(t)}{\rho_{b,a} D\left(L_{b,a}\chi'\left(T_{b,a}(t)\right) - C_p\right)} \tag{8}$$

Substitute equation (4) into (8), we obtain:

$$\frac{dT_{b,a}}{dt} = \frac{C_p J_{b,a}\left(T_{b,a}(t) - T_S\right)^{4/3}}{D\left(L_{b,a}\chi'\left(T_{b,a}(t)\right) - C_p\right)} \tag{9}$$

3.1.2 Crystallization in magma

In this modeling system, assume the crystals formed within the interior of magma are small enough to remain suspended in the turbulently convective magmas. Generally, the crystal content of magma is dependent on the magma temperature. Two ways to calculate the crystal content of magma are taken into account. The first one assumes that the crystal content of magma is proportional to the reciprocal of magma temperature, which is only suitable for basaltic magma and described as [*Huppert and Sparks*, 1988]:

$$\chi\left(T_b(t)\right)=\frac{7200}{T_b(t)}-6 \quad [1091\,°C < \mathrm{T_b} < 1200\,°C] \tag{10}$$

The second one assumes a linear relationship between the crystal content of magma and magma temperature [*Hort*, 1997].

$$\chi\left(T_{b,a}(t)\right)=\frac{T_L-T_{b,a}(t)}{T_L-T_S} \tag{11}$$

Equation (11) can be used for both basaltic and andesitic magmas. For both of the modeling methods, it can be seen that the crystal content of magma grows as the magma temperature $T_{b,a}(t)$ decreases. To further calculate equation (8), taking the first order derivative of $\chi(T_{b,a}(t))$ in (10) and (11) with respect to the magma temperature $T_{b,a}(t)$ lead to

$$\chi'\left(T_{b,a}(t)\right)=-\frac{7200}{T_{b,a}^2(t)} \tag{12.a}$$

$$\chi'\left(T_{b,a}(t)\right)=-\frac{1}{T_L-T_S} \tag{12.b}$$

3.1.3 The relationship between crystallization and viscosity

From equation (4), the heat flux $F_{b,a}(t)$ is affected by the magma viscosity. Also, it has been found that the magma viscosity is dependent on the crystal content of magma [*Roscoe*, 1952*; Lejeune and Richet*, 1995]:

$$\nu = \nu_0 (1 - \chi / \chi_c)^{-n} \tag{13}$$

where χ_c is the critical crystal fraction, beyond which flow is prevented (i.e., $\nu = \infty$), n is a constant.

Equation (13) reflects magma viscosity is a function of crystal content. As the mean temperature in the magma chamber moves towards the solidus temperature, the magma viscosity will increase greatly when crystallization is sufficient in the magma chamber. When crystal content approaches to the critical crystal fraction around χ_c, the viscosity approaches infinity. The final phase occurs when the basaltic/andesitic magma layer cools to a temperature at which there are sufficient crystals so that the magma viscosity becomes very large and resulting in convection ceases in the magma chamber. Therefore, the convection in magma system ceases when crystallinity reaches χ_c in this model.

Based on experimental and empirical evidence in [*Marsh,* 1981], the basic model selects χ_c = 60% and n = 2.5 as typical values. By this case, the viscosity becomes infinity as χ_c approaches 60%. For different types of magma, equation (13) can be reduced to [*Shaw*, 1980; *Marsh*, 1981]

$$v_b = 0.1(1 - 1.67\chi_b)^{-2.5} \tag{14.a}$$

$$v_a = 1.5(1 - 1.67\chi_a)^{-2.5} \tag{14.b}$$

$$v_{aw} = 0.3(1 - 1.67\chi_{aw})^{-2.5} \tag{14.c}$$

The relationship between the magma viscosity and the crystal content is shown in Figure 3.2, in which three different types of magmas are taken into account: basaltic magma, dry andesitic magma, and 3 wt% H_2O andesitic magma. It is the water content and the temperature of magma that lead to different viscosity properties. Water has the most dominant effect on the physical properties of the magma. Therefore, the determination of the water content of magma is vital to understanding the behavior of melts. In equation 12.c high water content decreases viscosity. In general, basaltic magmas are dry (i.e. H_2O less than 0.5 wt%) while andesites have higher water content. Basically, for a specific certain crystal content, the less water content and the lower temperature, the higher viscosity the magma has.

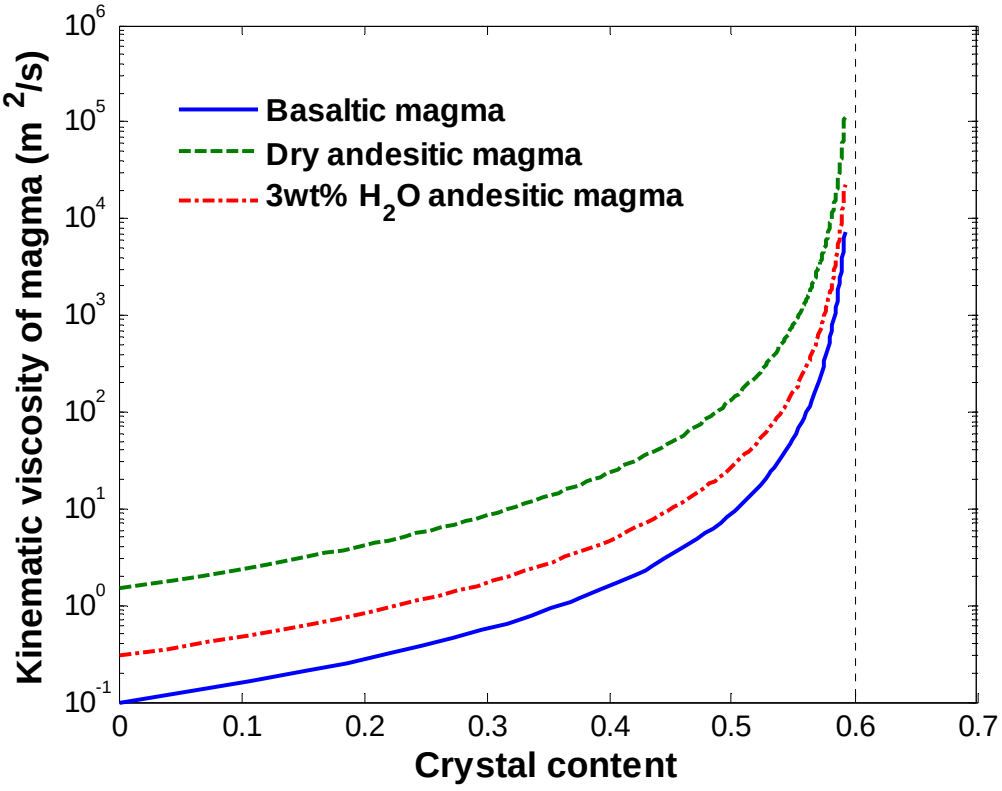

Figure 3.2: The relationship between magma viscosity and crystal content.

In Figure 3.2, with increasing of crystallinity the viscosity moderately increases but when a critical solid content is reached at ~ 60%, the viscosity increases so rapid that over a short range of crystallinity the magma behaves essentially as a solid. The vertical dash line at 60% shows the viscosity becomes infinite.

3.1.4 Crystals instantly settle on the floor of the magma chamber

In this section, I consider a somewhat different model from that of *Huppert and Sparks* [1988]. Here I assume that as the magma cools and crystallizes, crystals come out of suspension and accumulate on the chamber floor [Figure 3.3]. Denote by the initial depth of liquid magma D_0, $D_{b,a}(t)$ the depth of liquid magma at time t. The remaining magma is considered to be only liquid. Therefore, the viscosity of remaining magma $v_{b,a,aw}$ in convecting magma chamber is assumed to be a constant.

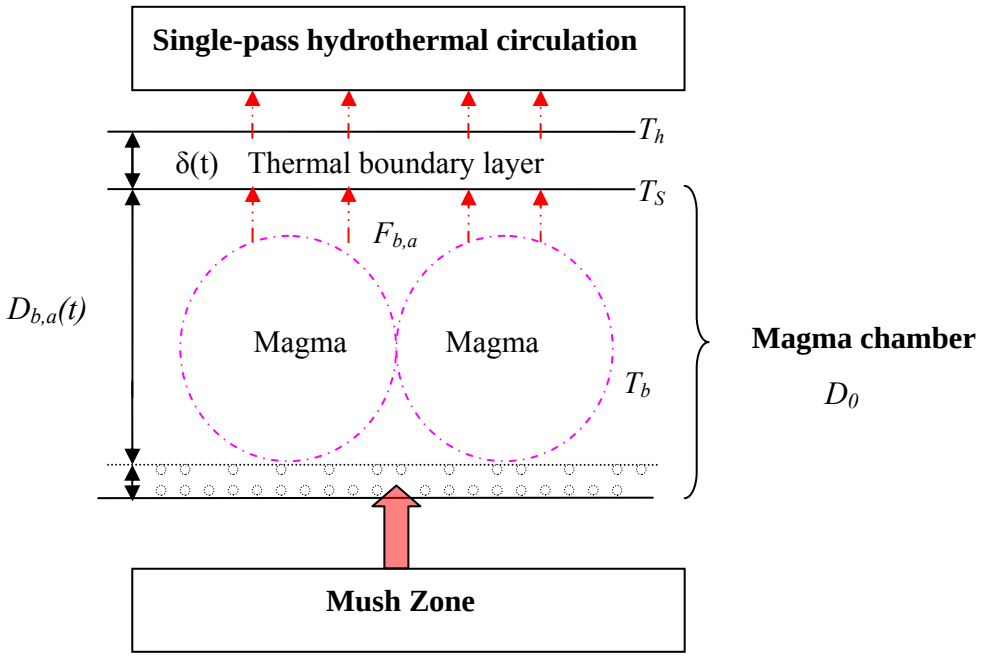

Figure 3.3: A convection magma chamber model with crystals settling.

The mass of liquid magma decreases with time as crystallization. Considering the mass of magma chamber is time-invariant, the mass of liquid magma is obtained:

$$M_{b,a}(t) = M - M_S(t) = \rho_{b,a} V_{b,a}(t) = \rho_{b,a} V - \rho_S V_S(t) \tag{15}$$

where $M_{b,a}$, M_S are the mass of liquid magma and mass of crystal; $V_{b,a}$ and V_S are the volume of liquid magma and crystal, respectively. It is worth pointing out, all these quantities are time varying.

Taking the first order derivative of equation (15) leads to:

$$\frac{dM_{b,a}}{dt} = -\frac{dM_S}{dt} = \rho_{b,a} A_m \frac{dD_{b,a}}{dt} = -\rho_S \frac{dV_S}{dt} = -\rho_S D_0 A_m \frac{d\chi(T_{b,a}(t))}{dt} \tag{16}$$

Combining equations (5) and (6), the new heat conservation equation in the magma liquid is obtained in this case:

$$C_p T_{b,a}(t) \frac{dM_{b,a}}{dt} + M_{b,a} C_p \frac{dT_{b,a}}{dt} + (1 - \chi(T_{b,a}(t)) L_{b,a} \frac{dM_{b,a}}{dt} - M_{b,a} L_{b,a} \frac{d\chi(T_{b,a}(t))}{dt} = -F_{ba} A_m \tag{17}$$

Substitute equations (15) and (16) into (17), we obtain:

$$-\frac{\rho_S}{\rho_{b,a}}C_p T_{b,a}(t)\rho_{b,a}D_0\chi'\frac{dT_{b,a}}{dt}+\rho_{b,a}D_0C_p\left(1-\frac{\rho_S}{\rho_{b,a}}\chi(T_{b,a}(t)\right)\frac{dT_{b,a}}{dt}$$
$$-\frac{\rho_S}{\rho_{b,a}}D_0(1-\chi)L_{b,a}\rho_{b,a}\chi'\frac{dT_{b,a}}{dt}-\rho_{b,a}D_0\left(1-\frac{\rho_S}{\rho_{b,a}}\chi(T_{b,a}(t))\right)\chi'\frac{dT_{b,a}}{dt}=-F_{b,a} \quad (18)$$

Therefore, the rate of magma temperature change can be finally expressed as:

$$\frac{dT_{b,a}}{dt}=\frac{-F_{b,a}}{\rho_S D_0\chi'\left(C_p T_{b,a}(t)+L_{b,a}(1-\chi(T_{b,a}(t))\right)+D_0\left(\rho_b-\rho_S\chi(T_{b,a}(t)\right)(\chi'-C_p)} \quad (19)$$

3.2 Hydrothermal circulation

The temperature of the hydrothermal fluid near the top of the magma body is much less than the melting point of magma. With heat transfer from the magma, it causes the magma to cool and crystallization inside of the magma chamber. As a result, the heat flux transport from the magma chamber decreases with time. Likewise, the temperature of hydrothermal system and heat flux decline with respect to time.

To express conservation of energy with a magma heat flux boundary condition, assume heat is transferred from a subsurface magma body with a horizontal area A_m to the base of the hydrothermal system by conduction across an impermeable thermal boundary layer $\delta(t)$. And the heat conducted from the magma through this conductive boundary layer is transferred by hydrothermal circulation to the seafloor, without conductive heat loss, where it discharges through the vent field area A_d. The heat balance equation can be written by [*Lowell and Germanovich*, 2004]:

$$F_{b,a}(t)A_m = F_h(t)A_d = \lambda \frac{T_S - T_h(t)}{\delta(t)} A_m \tag{20}$$

where λ is thermal conductivity factor. Therefore, equation (20) simply states that the heat conducted from the turbulently convecting magma body (A_m) into the base of the hydrothermal system equals to the heat carried to the bottom of the discharge zone (A_d) by hydrothermal advection.

Assume the hydrothermal system is operated at temperature $T_h(t)$. The heat flux in hydrothermal system can be obtained:

$$F_h(t) = \rho_f C_f u T_h(t) \tag{21}$$

Where ρ_f is fluid density, C_f is fluid specific heat and u is the Darcian upflow velocity.

For simplicity, assume the recharge zone temperature is zero and the flow resistance is dominated by the discharge zone [described more detail in *Lowell and Germanovich*, 2004]. Then this velocity is driven by buoyancy and expressed as:

$$u = \frac{\alpha_f g k T_h(t)}{v_f} \tag{22}$$

Where α_f is the coefficient of thermal expansion of fluid, k is permeability, v_f is the kinematic viscosity of fluid, respectively. Substitution equation (22) into (21) leads to:

$$F_h(t) = \rho_f C_f \frac{\alpha_f g k}{\nu_f} T_h^2(t) \tag{23}$$

Combing equations (20) and (23), we obtain the heat flux in magma transferred out by hydrothermal circulation:

$$F_{b,a}(t) = \frac{\rho_f C_f \alpha_f g k}{\nu_f} \frac{A_d}{A_m} T_h^2(t) \tag{24}$$

Correspondingly, the total heat output can be expressed as:

$$F_{b,a}(t) A_m = \frac{\rho_f C_f \alpha_f g k A_d}{\nu_f} T_h^2(t) = \gamma T_h^2(t) \tag{25}$$

where $\gamma = \frac{\rho_f c_f \alpha_f g k A_d}{\nu_f}$ is proportionality coefficient of hydrothermal temperature.

So far, I have discussed the theoretical basis for modeling the interaction between magma convection and hydrothermal circulation and introduced the heat flux activity driven by thermal convection in two cases, which are crystal in suspension and crystal settling, crystallization as a function of magma temperature and relationship between crystal content and viscosity. Fundamental equations are derived to describe the heat flux $F_{b,a}(t)$, total heat output $F_{b,a}(t)A_m$ and hydrothermal temperature $T_h(t)$ of these systems. Corresponding simulation results will be given in the following chapter.

CHAPTER 4

MODEL RESULTS AND DISCUSSION

4.1 Magma convection without replenishment

Figure 4.1 shows the total heat output $F_{b,a}(t)A_m$ from the convecting basaltic magma assuming two different formulas for the relationship between magma crystal content and temperature, respectively, as well as for two different areas A_m. Figure 4.2 also shows the total heat output, only for the different model, in which all crystals settle onto the chamber floor. The dotted lines in both figures located at 10^9 Watts and 10^7 Watts denoting the range of total hydrothermal heat output measured in hydrothermal systems at oceanic spreading center (see Table 1.1).

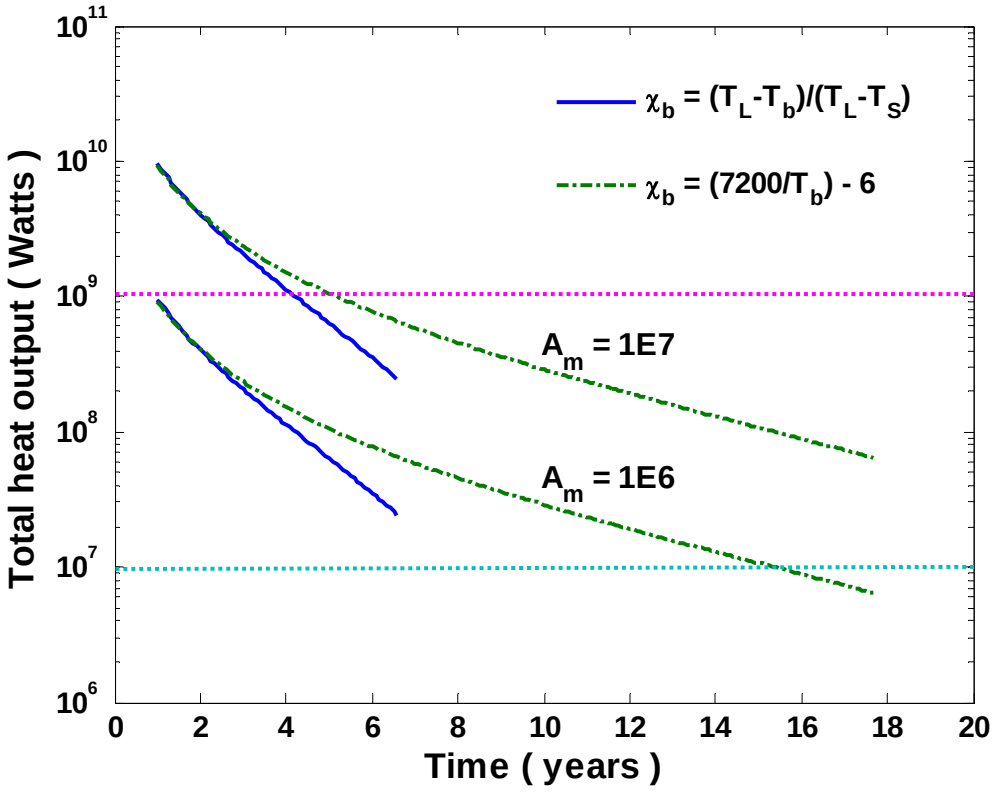

Figure 4.1: Total heat output from the convecting magma for crystals in suspension model without magma replenishment.

From Figure 3.2, crystallinity and viscosity increase as the magma temperature decreases. The Rayleigh number *Ra* also decreases and the amount of heat transferred into the hydrothermal system decreases correspondingly. In Figure 4.1, it is seen that the heat output from the magma chamber decreases rapidly in ten-year period. Two simulations show that the lifetime of the magma based on the *Hort* [1997] formula (equation (11)) is shorter than that using the *Huppert and Sparks* formula (equation (10)) for the relationship $\chi(T_{b,a})$ because it has lower final magma temperature when magma convection ceases as crystal approach to 60%. Area A_m only plays a role in determining the total amount of heat flux but has no influence on the lifetime of

magma convection. This is also indicated in equation (4).

From the model described in Section 3.1.4, all crystals come out of the liquid magma and settle onto the magma chamber floor. Compared with Figure 4.1, Figure 4.2 has the higher initial total heat output and the lower decay rate of hydrothermal system for both formulas. In this case, the lifetime of hydrothermal system is increased by several decades. For larger surface area A_m the lifetime approaches 70 years with a heat output more than 10^7 Watts.

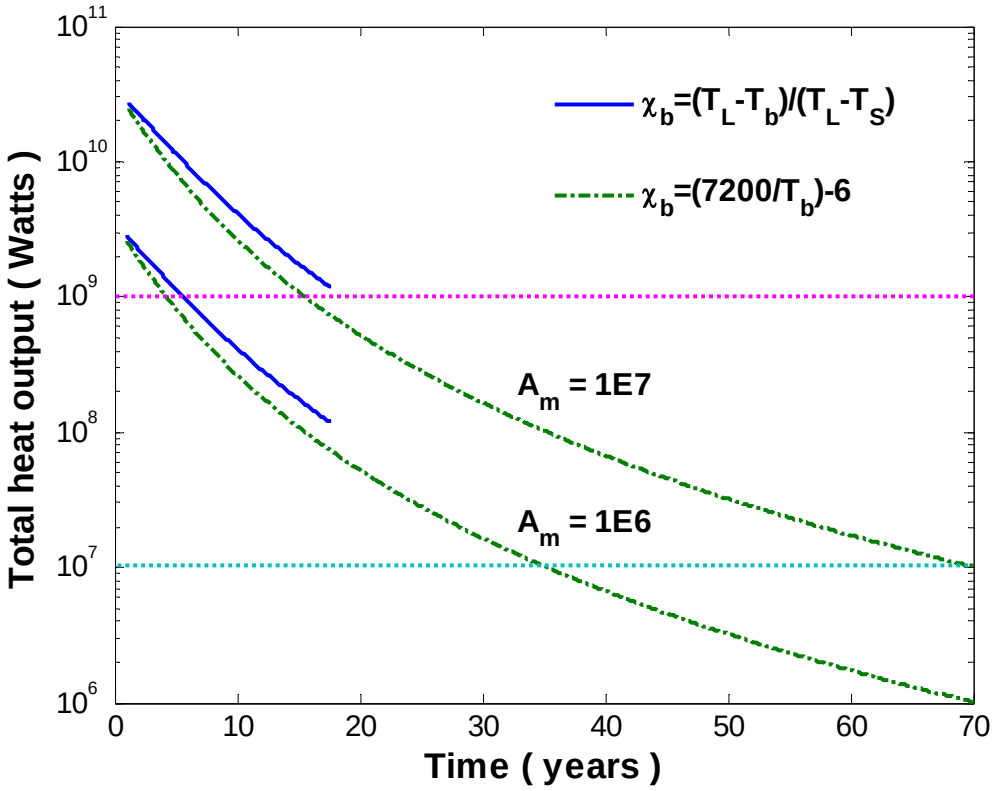

Figure 4.2: Same as Figure 4.1, except using crystals settling model for seventy years.

From Equation (1), the thickness of magma layer is the most significant

parameter affecting *Ra*. All crystals accumulate on the lower boundary layer in this case, which cause the available liquid magma depth decrease with time. Heat transport from the magma chamber decrease accordingly resulting in the slower decay of magma temperature and extend the lifetime of magma convection. However, the heat output still drop rapidly between 10^9 Watts and 10^8 Watts.

4.2 The behavior of the hydrothermal system

To further emphasize the implications of the heat output results given in Figure 4.1and 4.2, Figure 4.3 and 4.4 show the hydrothermal temperature with respect to time for different values of permeability k (i.e. different values of factor γ in equation (24) by changing other parameters). With increasing permeability k, the hydrothermal mass transport increases; but the temperature of hydrothermal system decreases because the total heat output is fixed. Thus although permeability k, which can be regard as a poorly known parameter, exerts significant control on hydrothermal vent temperature during this time interval, the most important feature of Figure 4.3 and 4.4 are that the hydrothermal temperature still decreases significantly.

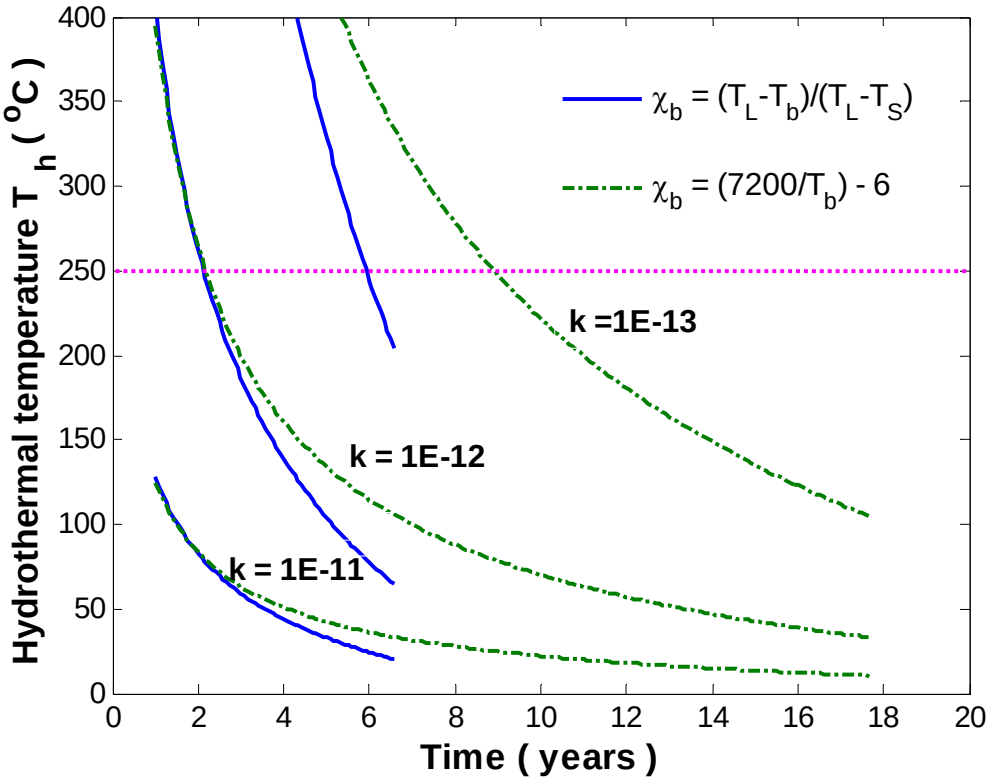

Figure 4.3: Hydrothermal system temperatures as a function of time for crystals in suspension model with different permeability *k*.

The temperature T_h = 250 °C denotes the lower limit for observed black smoker vent temperature. We notice that the temperature of hydrothermal system drops very quickly during the entire eighteen-year lifetime in Figure 4.3. Although in Figure 4.4, magma convection system is not dead within a hundred years because convection is driven only by liquid magma, the hydrothermal temperature still drops to a lower temperature rapidly in the first ten years.

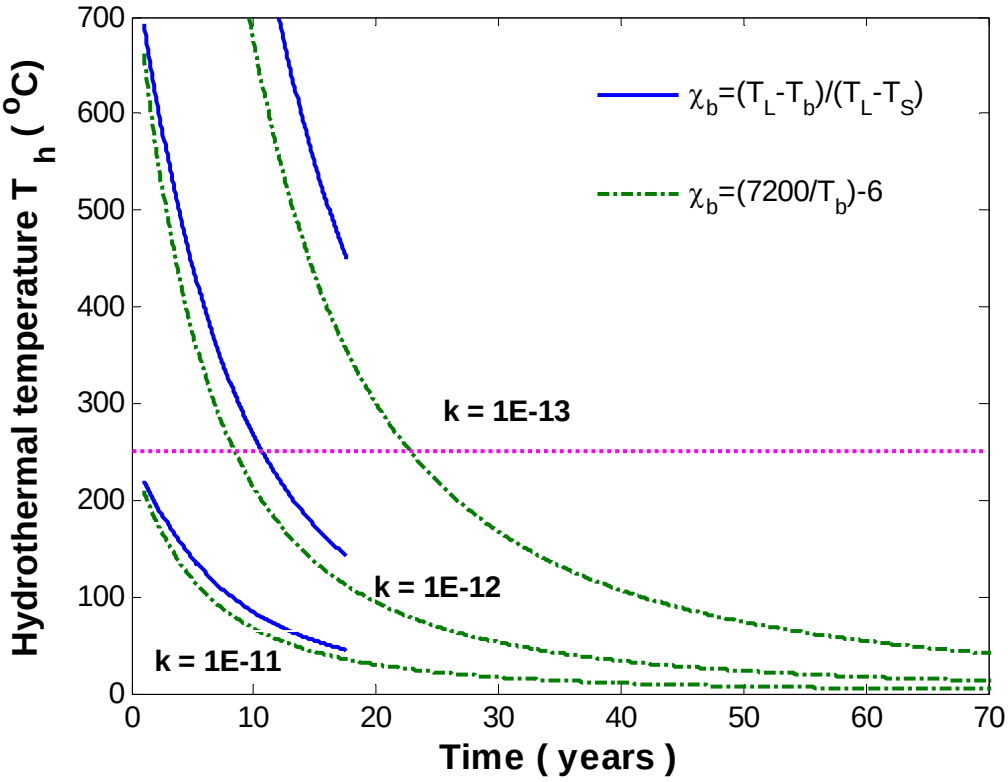

Figure 4.4: Same as Figure 4.3, except using crystals settling model.

Such rapid decay of a seafloor hydrothermal system is not commonly observed in long-lived system that are driven by basal magmatic heat sources; rather heat transport from the magma chamber maintains relatively steady vent temperatures and heat output. The basic model presented here suggests that magma convection alone may not be sufficient to maintain high hydrothermal temperature and heat output for decadal time scales. The inconsistency of above simulation results with the observations provides the motivation to develop magma convection models with replenishment. These will be introduced in Chapter 5.

4.3 Effect of magma solidus temperature

When the crystal content approaches to 60%, the magma convection ceases, at which the magma temperature is at 1092 ºC for *Huppert and Sparks* [1988] and 1123 ºC for *Hurt* [1997], respectively. The solidus temperature should be lower than those of two final magma temperatures, which allow magma system convection stop at that time. Different solidus temperatures of magma will affect the lifetime of magma convection. From equations (4) and (9), higher T_{bS} has lower amount of heat flux and lower decay of the magma chamber temperature. It can be seen that the convective activity lasts longer given higher temperature T_{bS}. If the T_S very close to these two values, magma temperatures drop very slowly and magma convections take very long time to cease. If choose a lower *Ts* (e.g 1040 ºC), the magma convection system decays very quickly. To keep the magma convection system functioning for a reasonable period the temperature 1070 ºC serves as a reasonable solidus temperature in this thesis. Moreover, from the results of *Maclennan* [2007], most of the latent heat is released before crystal fractions reaches 60%. Therefore, from the perspective of heat transport, the exact value for the solidus temperature is of little importance.

Figure 4.5 shows the influence of the solidus magma temperature T_{bS} on the lifetime of basaltic magma convection. Figure 4.6 shows the result at the beginning of hydrothermal system lifetime for the first 10 years. Figure 4.7 shows the similar result with different crystal content and magma temperature function.

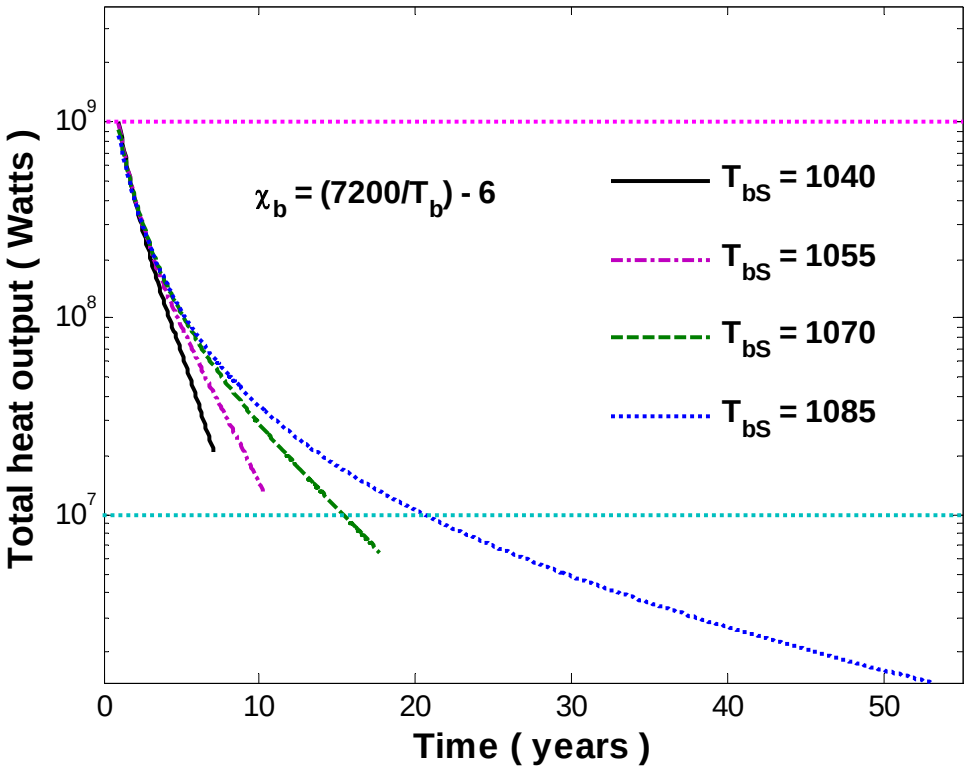

Figure 4.5: Effect of T_{bS} on the lifetime of magma convection during the entire period.

Figure 4.5 shows that magma system with higher T_{bs} gives hydrothermal system longer lifetime. However, if one considers 10^7 Watts as the lower value of hydrothermal heat flux, the temperature T_S will have slightly affection for the lifetime of magma convection.

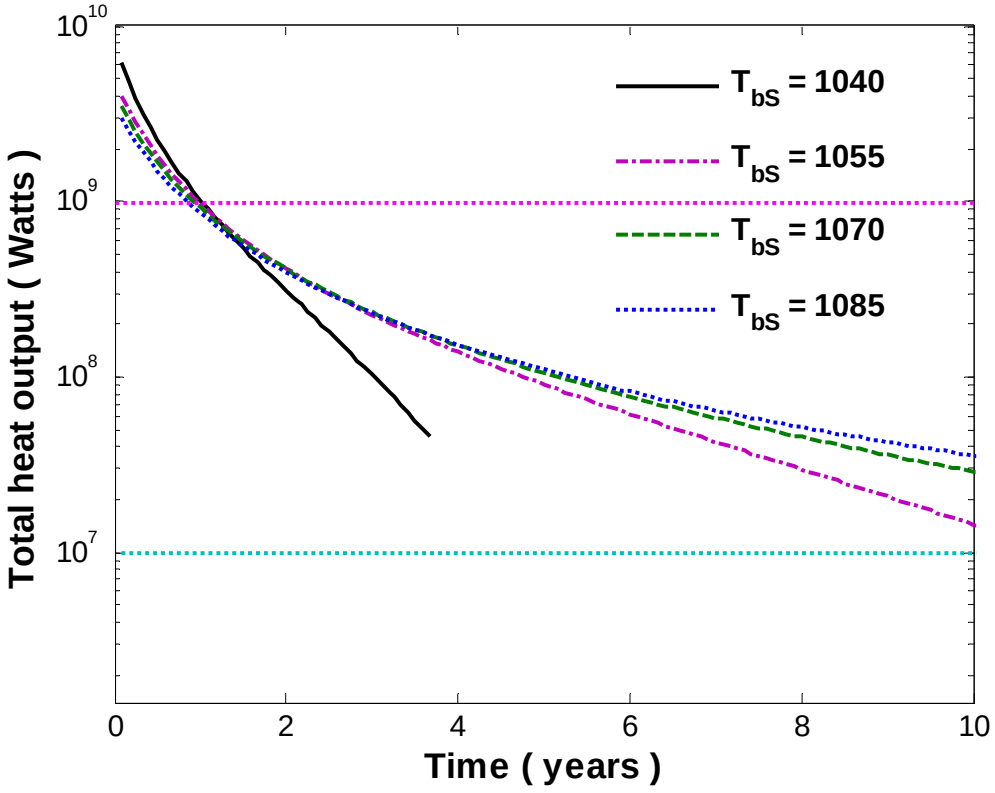

Figure 4.6: Effect of T_{bS} on the lifetime of magma convection over the first ten years using the same crystallinity function as in Figure 4.5.

From Figure 4.6, the lowest T_{bs} gives the highest total heat output at the beginning of one year. However, with the most rapidly decay of the magma chamber temperature, hydrothermal system with the highest initial heat output transport will have the shortest lifetime.

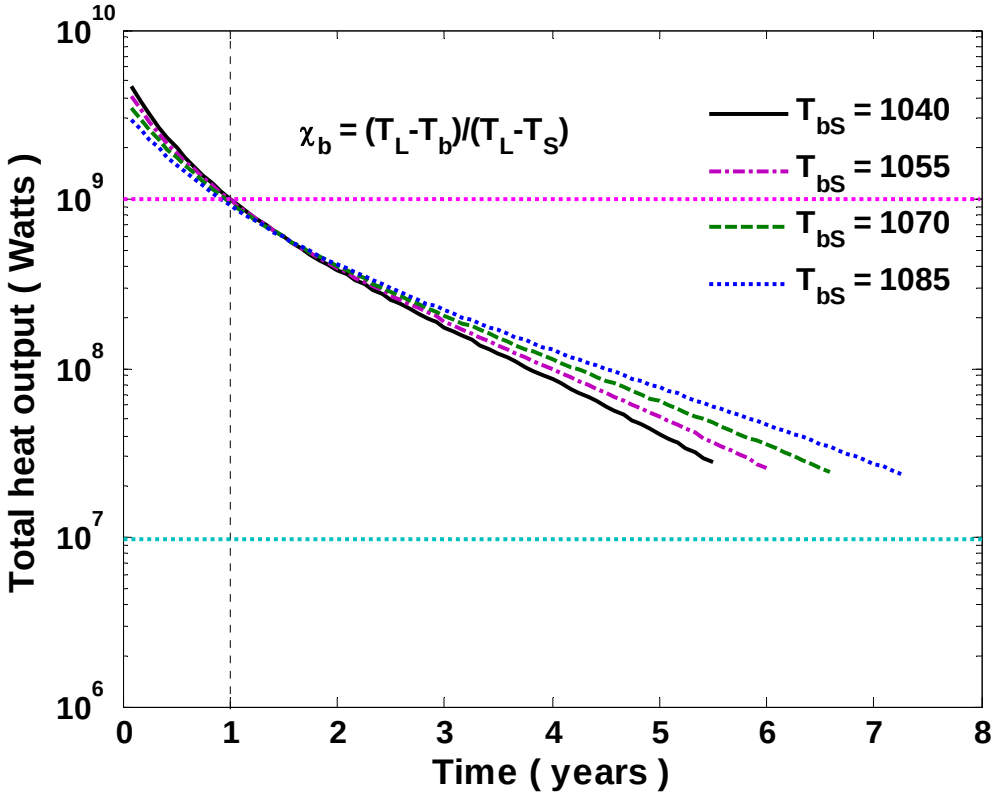

Figure 4.7: Same as Figure 4.5, except using the linear crystallinity expression as a function of magma temperature.

Compared with results shown in Figure 4.5, all hydrothermal systems with different T_{bs} in this case have a lower total heat output and shorter lifetime since the magma convection stops earlier due to rapid approach to 60% crystal content.

4.4 Comparison between basaltic and andesitic magma

One of the most active hydrothermal fields in the Lau back-arc basin was discovered in 1989 [*Fouquet et al.*, 1991]. High-temperature hydrothermal systems distributed along the Eastern Lau Spreading Center have characteristics that strongly contrast with those was found at normal mid-ocean ridges. One of the main differences results from the fact that some of the hydrothermal systems are hosted on

andesite [*Fouquet et al.*, 1991] and are driven by andesitic magma chambers [*Collier and Sinha*, 1992].

Andesitic magma has lower liquidus and solidus temperatures than those of basaltic magma [*Spera*, 2000]. Moreover, because andesite has higher water and SiO_2 content, andesitic magma has a greater viscosity and lower density than that of basaltic magma [*Spera*, 2000]. These factors affect the convective properties of the magma and hence may affect the heat output to the overlaying hydrothermal system.

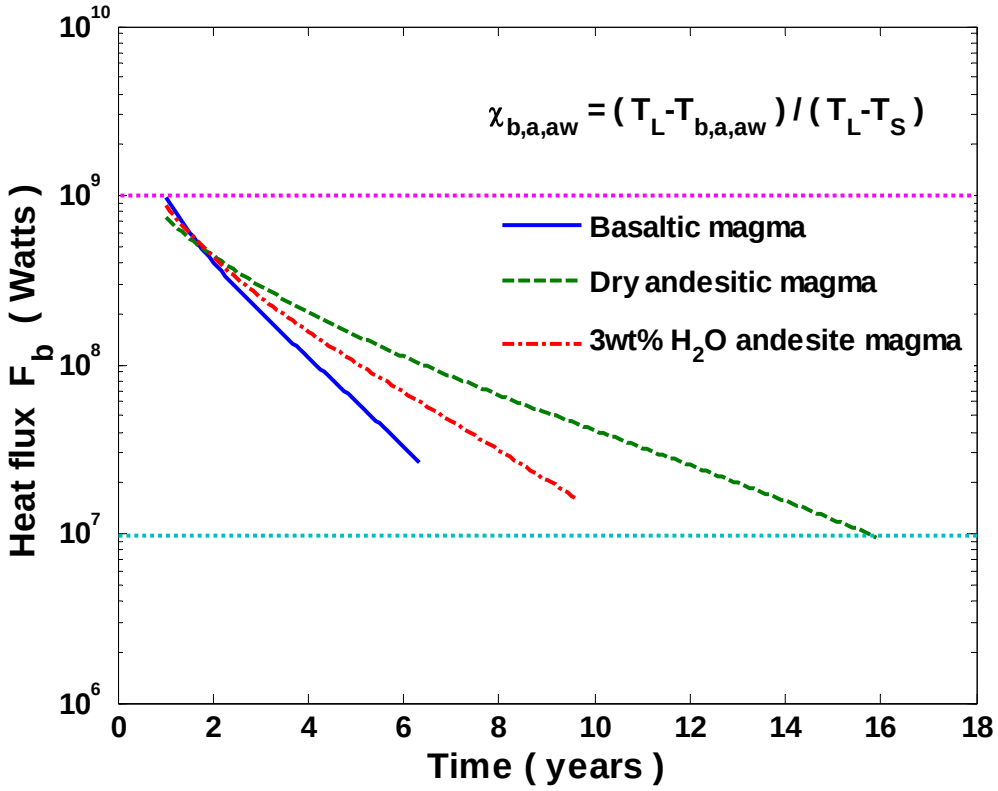

Figure 4.8: Comparison the total heat output among basaltic, dry and wet andesitic magma.

Figure 4.8 shows that the hydrothermal systems driven by the greater viscosity

of andesitic magma might undergo a slower decline than basaltic ones, however, the magma convection system lifetime about ten years. Since higher viscosity andesitic magma has convections less vigorously than basaltic magma does in the same dimensioned magma chamber, it provides slower heat transport and slower rate of vent temperature decay.

CHAPTER 5

MAGMA CHAMBER REPLENISHMENT

As the magma begins to cool and crystallize, the volume occupied by the magma decreases because the crystals have greater density than liquid magma. If the elastic response of the surrounding rock is neglected, the internal pressure declines, which would result in magma transport from the underlying mushy zone into the magma chamber. The additional heat supply from magma replenishment may help maintain heat transport from the convecting magma to the hydrothermal system [*Lowell and Germanovich*, 1994; *Humphris and Cann*, 2000]. Two cases are taken into account in this Chapter. In the first scenario, the overall magma chamber volume will remain unchanged; in the second scenario, the magma volume is assumed to grow as the fresh magmas are added.

5.1 Fixed Volume of Magma chamber

Let ρ_S be the density of gabbro (crystal); V_L the volume of liquidus magma at the initial stage. Define $V_m(t)$ to be the volume of the magma-crystal mixture during the cooling and crystallization. Thus, at time t, the volume of the crystal is $V_m(t)\chi(T_{b,a}(t))$, while the volume of the liquidus magma is $V_m(t)(1-\chi(T_{b,a}(t)))$. From the law of mass conservation, we obtain:

$$V_m(t)\chi\left(T_{b,a}(t)\right)\rho_S + V_m(t)\left(1-\chi\left(T_{b,a}(t)\right)\right)\rho_{b,a} = \rho_{b,a}V_L \tag{26}$$

Recalling a rectangular magma body of area A_m, depth D and $V_L = DA_m$, the volume of the magma-crystal mixture is obtained:

$$V_m(t) = \frac{DA_m}{\left(1 - \chi\left(T_{b,a}(t)\right)\right) + \frac{\rho_S}{\rho_{b,a}}\chi\left(T_{b,a}(t)\right)} \tag{27}$$

Correspondingly, the rate of the magma-crystal mixture volume change at time t can be expressed as:

$$\frac{dV_m}{dt} = \frac{DA_m\beta}{\left(1 + \chi\left(T_{b,a}(t)\right)\beta\right)^2}\frac{d\chi(T_{b,a})}{dT_{b,a}}\frac{dT_{b,a}}{dt} \tag{28}$$

where $\beta = \frac{\rho_S - \rho_{b,a}}{\rho_{b,a}}$.

Assuming fresh and crystal-free liquidus magma with temperature T_L fills up the free space in the magma chamber generated by crystallization of original magma. The additional heat flux input resulting from magma replenishment is defined as:

$$\begin{aligned} F_r(t) &= \rho_{b,a}(C_pT_L + L_{b,a})\frac{dV_m}{dt}\frac{1}{A_m} \\ &= \rho_{b,a}(C_pT_L + L_{b,a})\frac{D\beta}{\left(1 + \chi\left(T_{b,a}(t)\right)\beta\right)^2}\chi'\left(T_{b,a}(t)\right)\frac{dT_{b,a}}{dt} \end{aligned} \tag{29}$$

Taking into account the heat input resulting from magma replenishment given by equation (29), the heat balance equation (7) is modified as:

$$\rho_{b,a}C_pD\frac{dT_{b,a}}{dt}-\rho_{b,a}L_{b,a}D\chi'\left(T_{b,a}(t)\right)\frac{dT_{b,a}}{dt}+C_pT_{b,a}\rho_{b,a}\frac{dV_m}{dt}$$
$$+(1-\chi(T_{b,a}(t))L_{b,a}\rho_{b,a}\frac{dV_m}{dt}=-F_{b,a}(t)+\xi F_r(t) \quad (30)$$

Compared with equation (7), the second term on the right hand side of equation (30) represents the magma replenishment as a new heat source. Equation (30) assumes that the fresh magma is immediately fully mixed with the existing magma. The factor $\xi \geq 0$ is introduced to indicate the amount of magma replenishment. Specifically, $\xi = 0$ indicates no replenishment, at which point equation (30) is reduced to equation (7). When $\xi = 1$, the amount of replenishment compensates the exactly same amount of decrease in volume of magma-crystal mixture due to crystallization.

Combing equations (29) and (30), the rate of temperature change of the magma becomes:

$$\frac{dT_{b,a}}{dt}=\frac{F_{b,a}(t)}{\rho_{b,a}D(L_{b,a}\chi'\left(T_{b,a}\right)-C_p)+\xi\rho_{b,a}D(C_p(T_L-T_{b,a})+\chi(T_{b,a})L_{b,a})\chi'\left(T_{b,a}\right)\frac{\beta}{(1+\chi\left(T_{b,a}\right)\beta)^2}} \quad (31)$$

From equations (4) and (31), we get a new replenishment model for the magma temperature and heat output that drives the hydrothermal system.

5.2 Magma chamber grows upon replenishment

In this section, the volume of chamber is allowed to increase during the

magma replenishment process. Assume the thickness of magma chamber remains constant, which results in a time-varying area of magma chamber. Let $A_m(t)$ denote the area of magma chamber at time t, the corresponding volume of magma chamber is represented by:

$$V(t) = DA_m(t) \tag{32}$$

Now the volume of magma chamber is time varying. The heat content of a volume of magma is described:

$$H(t) = (\rho_{b,a} C_p T_b + (1-\chi)\rho_{b,a} L_{b,a}) V(t) \tag{33}$$

In contrast to the previous section, the heat flux due to the magma replenishment is described as:

$$F_r = (\rho_{b,a} C_p T_L + \rho_{b,a} L_{b,a}) u(t) \tag{34}$$

where $u(t)$ denotes the velocity of the incoming magma, which is assumed to be crystal-free magma at its liquidus temperature. Assume the magma enters from below across an area $A_b(t)$. In analogy to equation (6), the heat conservation in the magma liquid layer across the interface leads to

$$\frac{d\left((\rho_{b,a}C_pT_{b,a}(t)+\left(1-\chi\left(T_{b,a}(t)\right)\right)\rho_{b,a}L_{b,a})DA_m(t)\right)}{dt}=-F_{b,a}(t)A_m(t)+F_r(t)A_b(t) \qquad (35)$$

where the second term on the right hand side of equation (35) represents the heat transfer due to magma replenishment, in which the area terms increase with magma replenishment as a time function.

Expanding the derivative terms on the left hand side of equation (35) leads to

$$\begin{aligned} &V(t)\frac{d\left((\rho_{b,a}C_pT_{b,a}(t)+(1-\chi)\rho_{b,a}L_{b,a})\right)}{dt}+(\rho_{b,a}C_pT_{b,a}(t)+(1-\chi)\rho_{b,a}L_{b,a})\frac{dV}{dt} \\ &\quad =-F_{b,a}(t)A_m(t)+F_r(t)A_b(t) \end{aligned} \qquad (36)$$

To solve equation (36), an expression for $A_m(t)$ is necessary. From mass conservation, one obtains:

$$\frac{dm}{dt}=\rho_{b,a}\frac{dV}{dt}+V\frac{d\rho}{dt}=\rho_{b,a}A_b(t)u(t) \qquad (37)$$

In contrast to the model in the preceding section, the term $V\frac{d\rho}{dt}$ can be neglected because the mass of magma added to the magma chamber is much more than is needed to maintain the magma chamber volume, such that the density changes is ignorable. Assuming that magma replenishment occurs over the whole area, so that $A_b(t) = A_m(t)$, then equation (37) can be rewritten as :

$$\frac{dV}{dt} = D\frac{dA_m}{dt} = A_m u(t) \tag{38}$$

Assuming that the fresh replenished magma mixes into the magma chamber rapidly, the rate of the magma temperature changing can be obtained by substituting equations (32) and (38) into (36):

$$\frac{dT_{b,a}}{dt} = \frac{F_{b,a}(t) - \rho_{b,a}u(t)\left(C_p\left(T_L - T_{b,a}(t)\right) + \chi\left(T_{b,a}(t)\right)L_{b,a}\right)}{D\rho_{b,a}\left(\chi'\left(T_{b,a}(t)\right)L_{b,a} - C_p\right)} \tag{39}$$

In the following, two different models of replenishment velocity are proposed. First, magma replenishment occurs at a constant velocity for certain time period:

$$\begin{aligned} u(t) &= u_0 \qquad (0 < t < 10^9 s \approx 30 years) \\ u(t) &= 0 \qquad (t > 10^9 s) \end{aligned} \tag{40}$$

The area of magma can be obtained by integrating equation (38)

$$A_m(t) = A_{m0}e^{\frac{u_0 t}{D}} \tag{41}$$

where A_{m0} is the initial area of the magma chamber.

Alternatively, the velocity of replenishment is modeled as an exponential decay:

$$u(t) = u_0 e^{-bt} \tag{42}$$

where u_0 is the initial velocity. Similarly, the area of magma is obtained as:

$$A_m(t) = A_{m0} e^{\frac{-u_0 e^{-bt}}{bD}} \tag{43}$$

With modeling of magma area $A_m(t)$, the magma temperature and heat flux of magma system can be obtained through equation (39).

5.3 Numerical results

5.3.1 Fixed volume of magma chamber

The lifetime of magmatic heat transfer (Figure 4.1 and 4.2) and the high-temperature hydrothermal system (Figure 4.3 and 4.4) are significantly shorter than observed. Moreover, the heat output decays rapidly with time throughout the life of the system. Consequently, I consider whether magmatic heat replenishment from the underlying mush zone will significantly extend the life of the system.

In section 5.1, the volume of magma chamber was assumed to be constant. However, the volume of magma decreases due to the cooling and crystallization. The pressure of magma chamber decreases correspondingly, because the density of crystals is greater than that of liquid magma. The decrease of pressure drives new magma into the chamber from the underlying mush zone, thus maintaining the heat and pressure in the magma chamber. Rather than address this complicated dynamical process, for simplicity, I assume new liquid magma is simply added at a fixed rate.

***Basaltic magma (with crystal in suspension)*:**

Figure 5.1 depicts the total heat output $F_{b,a}(t)A_m$ as a function of time for two different replenishment rates controlled by the parameter ξ. Case 1 is for full replenishment, in which the rate of magma replenishment is the same as the rate of magma volume decrease resulting from crystallization. In case 2, higher rate replenishment is taken into consideration. ξ = 10 indicates that the rate of replenishment is ten times the rate of magma volume decrease. As before, Figure 5.1 also considers two different formulas for the relationship between the crystal content and magma temperature.

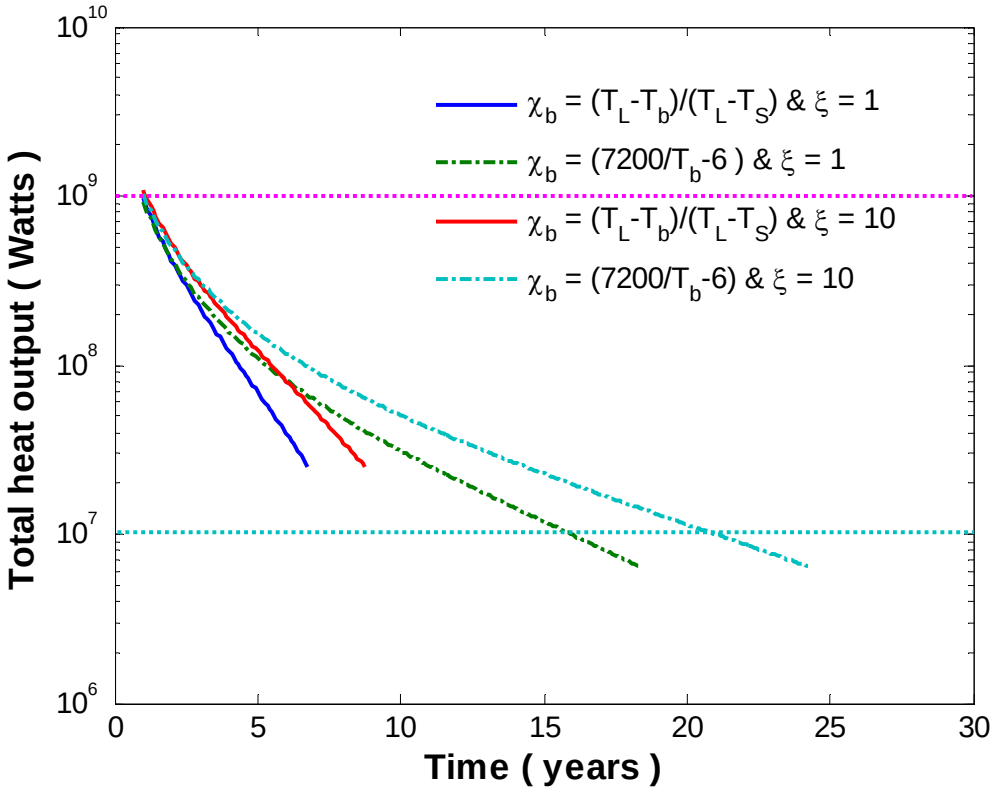

Figure 5.1: Total heat output at different rates of magma replenishment without magma chamber volume changing.

Figure 5.1 shows that full replenishment can not extend the lifetime of magma significantly compared to that without replenishment (Figure 4.1). Moreover, even in the optimum case of higher rate replenishment where the lifetime is only extended for few years longer.

***Andesitic magma*:** Based on the theoretical analysis, if andesite and basalt with the same replenishment rate, the cooler andesitic magma with larger viscosity causes additional magma volume to be less than that required by a basaltic magma for a given chamber size. Figure 5.2 shows that andesitic magmas-driven hydrothermal systems have lower peak of heat output than basaltic magmas.

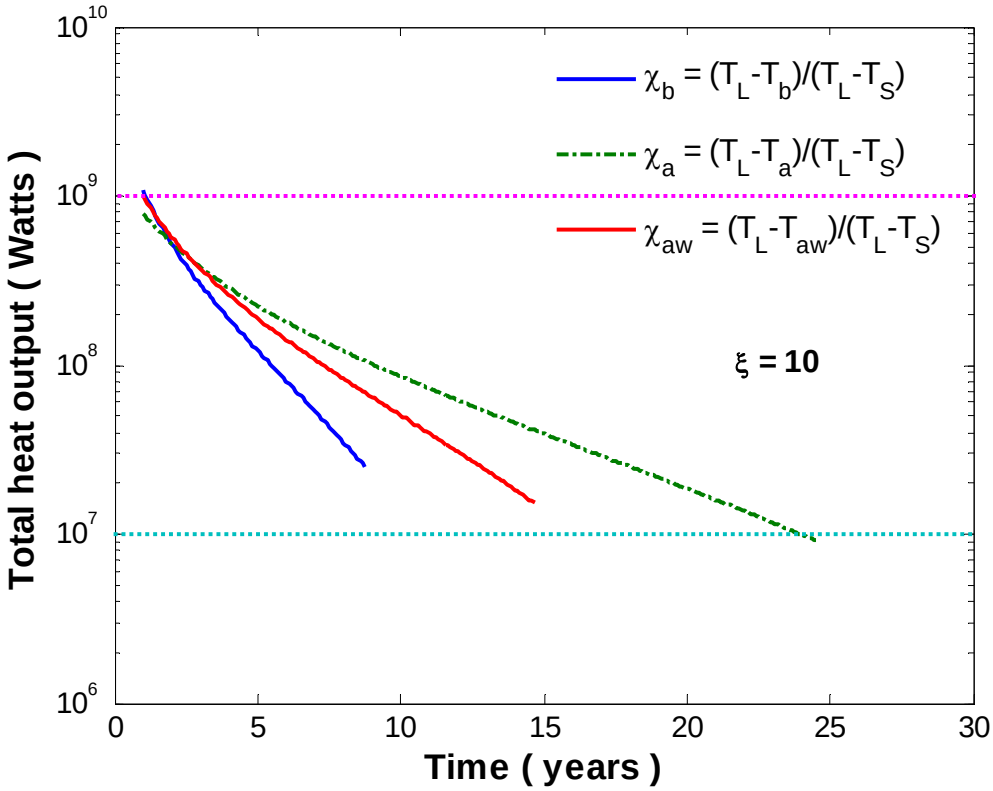

Figure 5.2: Total heat output with the replenishment factor $\xi = 10$ for three types of magma without magma chamber volume changing.

However, it is hard to say if andesitic magma has a longer lifetime because their higher viscosity makes andesitic magma more difficult for replenishment from the underlying mush zone. From the observation, Vigorous high-temperature black and white smokers were discovered at Vai Lili field on the northern section of the central VFR [*Fouquet et al.*, 1991, 1993]. However, the latest survey showed the hydrothermal activity here had declined significantly since the last survey in 1989 and most of hydrothermal vent field were covered by the eruption volcanism [*Fretzdorff et al.*, 2006]. It is possible that it is in a state where melt from the magma chamber has mostly crystallized (e.g., <30% melt) or it has not yet received a new replenishment of fresh magma or the lava covered all hydrothermal venting, however, these hypotheses need to be tested against observations.

5.3.2 Magma chamber volume increases with time

From the above simulation, we find that with even a ten fold volume increase of magma replenishment into the magma chamber does not significantly affect the lifetime of hydrothermal activity. Moreover, the model appears erroneous because it is unlikely for the magma chamber to remain constant if it is replenished at a rate 10 times greater than the rate of magma volume decrease from crystallization. In other words, the magma chamber should not be able to accommodate ten times amount of mass of magma initially in the chamber. If the hydrothermal activity is to maintain a steady state for twenty or thirty years as seems to be observed at many sites, the rate at which magma is filled into the magma chamber to provide enough heat flux and maintain hydrothermal system must be greater than assumed in the previous section.

Then the volume of the magma chamber must increase with time.

First, I assume the magma chamber is replenished with a constant velocity as in equation (40). Since black smokers with stable high temperature and heat output last for decades, we stop the simulations at thirty years. Simulations will show the rate curve of hydrothermal temperature and total heat output during this time interval. Figure 5.3 depicts the total heat output of magma system with different constant replenishment velocity.

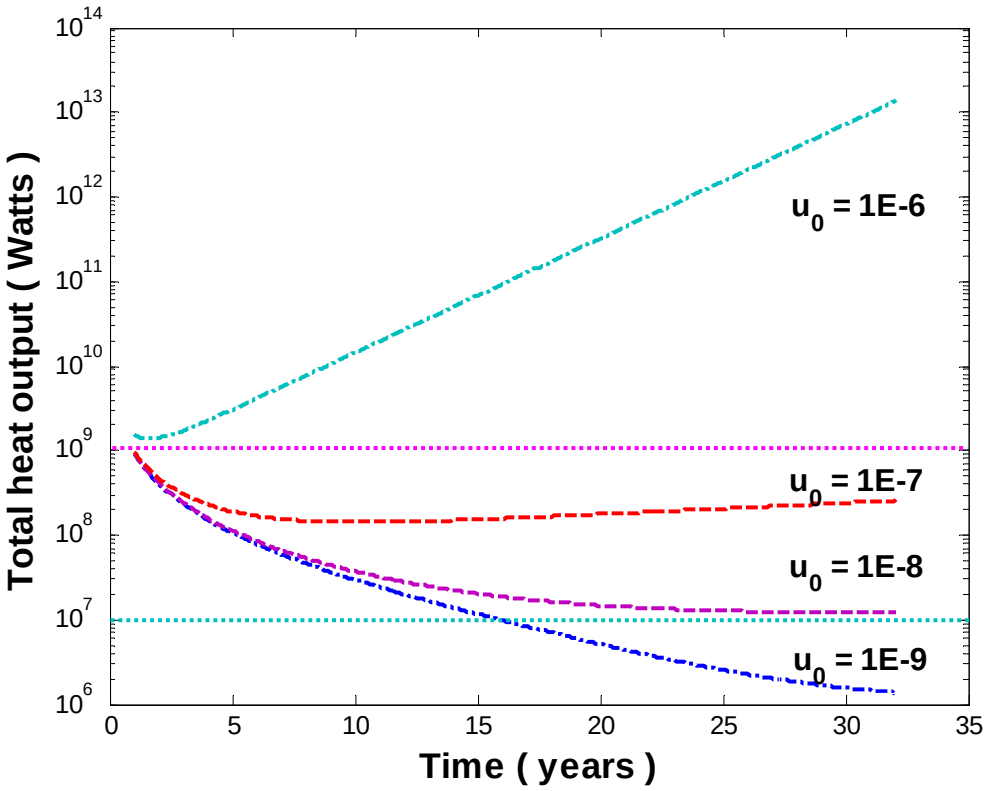

Figure 5.3: Total heat output with constant replenishment velocities for thirty years with magma chamber volume changing.

With velocity of 10^{-7} m/s and 10^{-8} m/s, the heat output of magma system is

between 10^7 Watts and 10^9 Watts, which is in the range of heat output typically observed. However, the velocity of 10^{-6} m/s and 10^{-9} m/s results in total heat output going out of the observation range, which indicates the unrealistic selection of velocity. Given a lower velocity, it cannot help to maintain hydrothermal system; while given a higher velocity, it will cause a magma eruption. Given an appropriate velocity, the model can effectively maintain a near steady heat output and the activity of hydrothermal system on the order of decades.

From another perspective, the observed magma chamber size is commonly less than $2x10^3$ m across-axis and often ~ 10^3 m along-axis [*Kent et al.*, 1990; *Detrick et al.*, 1993; *Collier and Sinha*, 1990]. For this reason, I carry out simulations with the chamber size as the stopping condition. Figure 5.4 shows the heat output of magma system with a constant replenishment velocity and with the magma chamber allowed to grow from 10^6 m^2 to $2x10^6$ m^2. Similarly, two models of relationship between crystal content and magma temperature are adopted. The lifetime of magmatic activity in both cases can be extended to about 25 years with the chamber replenishment.

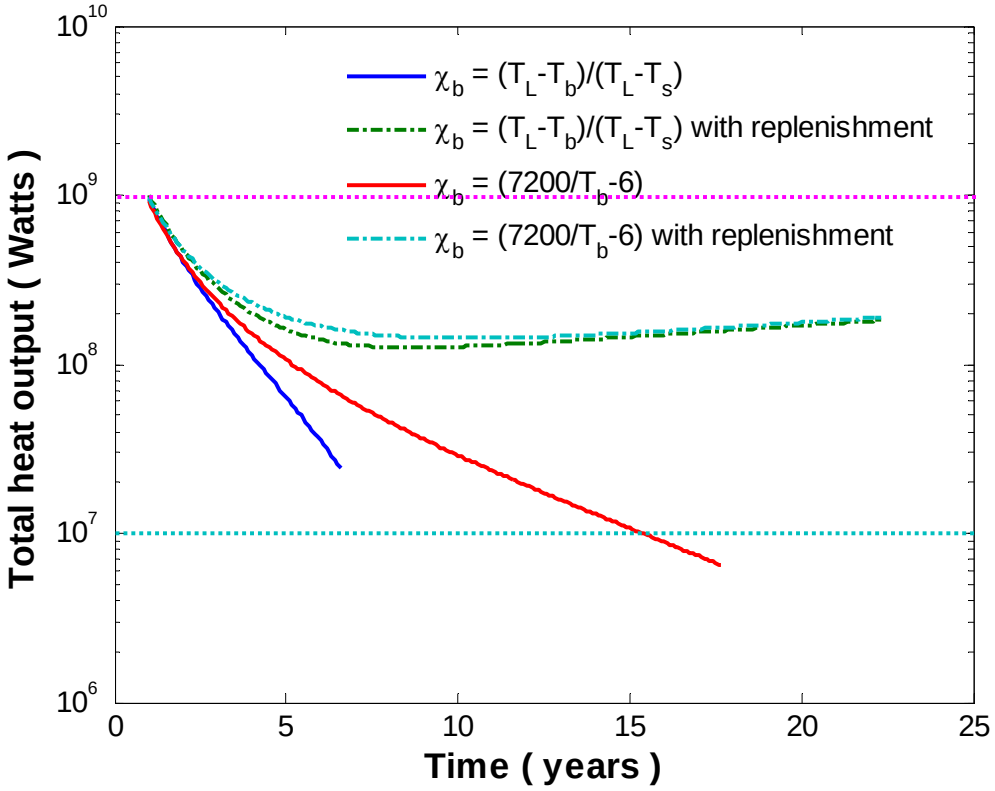

Figure 5.4: Total heat output with constant replenishment velocity 10^{-7} m/s until magma chamber volume equals $2x10^6$ m^2.

Combination of Figure 5.3 and 5.4 illustrate with appropriate model parameter (velocity to be 10^{-7} m/s in our example, while for velocity to be10^{-8} m/s, the magma chamber area is never larger than $2x10^6$ m^2), we can extend the lifetime of magma chamber activity to around 25 years. By this case, the heat output of hydrothermal system is between 10^7 Watts and 10^9 Watts, and the maximum of chamber size reaches $2x10^6$ m^2, which justifies the effectiveness of our magma replenishment modeling.

For the magma replenishment modeling in section 5.3, exponential decaying velocity can be also applied besides the constant velocity. Figure 5.5 shows the output of hydrothermal system with certain parameter sets. The lifetime of the hydrothermal activity can be extended to the desired value for both of the *Huppert and Sparks* [1988] and *Hort* [1997] formulas for $\chi(T)$. Moreover, the choice of formulas for $\chi(T)$ has a little influence on the lifetime of hydrothermal system.

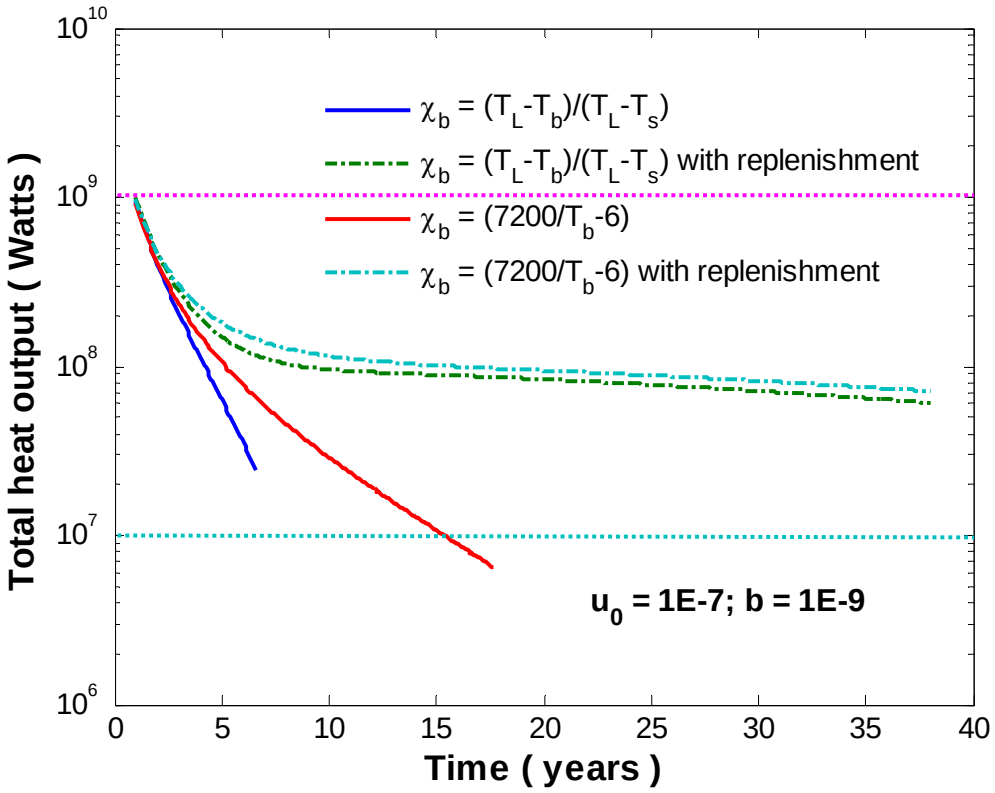

Figure 5.5: Same as Figure 5.4, except use the exponential replenishment velocity.

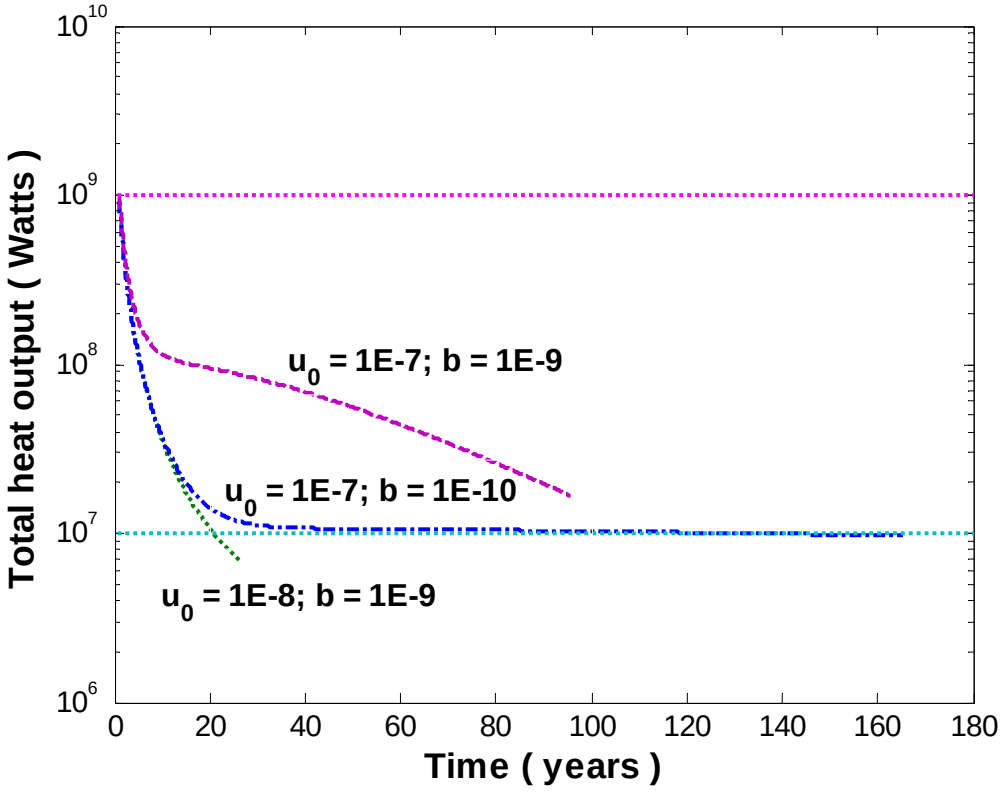

Figure 5.6: Total heat output with various exponential replenishment velocities.

Figure 5.6 also depicts the effects of parameter selection on the characteristics of hydrothermal system activity. It can be seen that different parameter selections can lead to different rate of heat output decrease. Therefore, the exponential decaying velocity modeling can effectively serve as the purpose of describing the hydrothermal system, and different parameter can be chosen to meet to requirement of different real systems.

5.4 Discussion

An improved model of convective magma heat transport has been demonstrated by simulation results in previous sections. With modeling the magma

replenishment process, the lifetime and heat transport of magma convection is extended to the value consistent with the observations. Although the model simulations suggest that magma replenishment coupled with magma chamber growth can help maintain a quasi-steady-state hydrothermal system, the models invoke a number of simplifications that need to be examined.

1. Magma chamber growth is assumed to be simple. The imaged seismic structures of the axial magma chamber are not taken into account when the magma chamber size grows across the axis. In reality, it appears that the magma chamber growth is closely related to the elasticity and stress field of the surrounding rock. Moreover, the magma chamber growth and pressurization of the magma cavity could lead to failure and magmatic eruption.

2. In the proposed model, I simply assume heuristic models for magma replenishment rate, which is justified by meeting the requirements of magma volume changes due to the crystallization. During the magma replenishment procedure, magma may not be transported from mush zone to the magma chamber at a constant velocity or according to any simple mathematical function. Pressure of magma chamber plays a significant role to determine the rate changes. To obtain a more realistic model of magma replenishment, the replenishment rate models need to link to geodynamics of magma chamber.

3. The effects of replenishment on magma chamber dynamics are greatly oversimplified. When the new crystal-free magma replenishes from underlying mush zone and mixes with the original magma, I assume instantaneous mixing regardless of

the mixing process. This also leads to instant equilibration. However, the replenished magma is composed of different temperature and chemical compositions compared with the magma present at the chamber at any given time. The chemical and physical differences may have an impact on the magma convection and crystal settling.

4. Magma chamber dynamics that do not incorporate replenishment are also greatly oversimplified. First, in addition to thermal convection, compositional convection can also affect crystal settling processes. However, in the 0-D thermal convection model, the complex convection dynamics is not considered. Second, after the magma crystallized, crystal suspension or instant settling is assumed without considering crystal attachment to roof. Actually, models need to be more complex and include details of crystal growth, settling, and the feedback on viscosity.

CHAPTER 6

CONCLUSIONS AND RECOMMENDATIONS FOR FURTHER WORK

In this thesis, I linked high-temperature seafloor hydrothermal systems to heat transfer from the underlying layer of vigorously convecting basaltic or andesitic magma. I considered a homogeneous thermal convection model in which crystals either stay suspended in the magma as they form, or alternatively, instantly settle down to the floor of the magma chamber. During the magma crystallization, the crystal content accepts two models in term of magma temperature. Moreover, a different viscosity model is assumed for different magma systems as a function of the water content of magma. Two models of the magma convection system with and without magma replenishment are considered.

By examining the magma convection system modeling without replenishment, the results of the numerical simulations show that systems were short-lived and heat output declined rapidly with time. However, real observations of seafloor hydrothermal systems indicate stable heat output and temperatures which remain near constant for decades. Therefore, I investigated the role of magma chamber replenishment.

To model the magma replenishment with all crystal suspension interior of magma, two schemes of magma chamber size assumption were adopted. First, the magma chamber is assumed to be fixed and the new magma fills at a constant rate. The amount of magma replenishment is selected to be the same as or ten times of the

magma volume decrease. Simulation results show that both cases do not significantly extend the lifetime of turbulent magma convection and the hydrothermal system heat output.

Second, I consider the case in which the volume of magma chamber is considered to grow during the stage of magma replenishment. The chamber depth is assumed to be constant, thus the growing chamber volume is due to the growing chamber area. I proposed two models to describe magma replenishment rate, a constant and exponential decay. The simulations show that both of the methods have been justified by simulation to extend the heat output and the lifetime of the hydrothermal systems are reasonable values. Hydrothermal systems driven by andesitic magma with the same rate of magma replenishment tend to have somewhat lower heat output than systems driven by basaltic magma because andesitic magma has greater viscosity (three times for dry andesite and fifteen times for 3 wt% andesite).

As discussed in Chapter 5, the models developed in this thesis are highly oversimplified. Future work would entail removing these simplifications. These include (1) mechanics of magma growth, (2) mechanics of magma flow and replenishment, (3) magma chamber dynamics. Actually, either the convecting magma body or the hydrothermal system circulation consists of complicated dynamics. Hydrothermal system with magma replenishment extends the lifetime by buffering the heat loss, depending on the fluid properties and dynamics of the magmas involved. To develop more realistic replenishment model for the homogeneous magma chamber by

the rapid injection of hot, relatively less dense, fresh magma, it is necessary to understand additional complexities of the process of magma transfer within the lower crust and how this transfer is linked to the evolution and replenishment of the melt lens.

In addition, the model makes predictions that can be tested by field observations. Repeated seismic surveys would help test whether the model of magma chamber growth is reasonable. Seismologic data reveals the geological structure of axis magma chamber. It provides the estimation about the crystal content, distribution, and its seismic properties derived from composition and microstructure of a melt body. From different microstructure, it can tell whether crystals suspend in the melt or form a crystallized floor. More realistic models of replenishment might also predict how compositions of eruptive lavas might change over time. Geochemical data illustrates short and long-term changes in magma composition, shallow magma transfer and eruptive behavior. It entails more details about how the new hot magma mixes with primitive cold magma mixture and more information about the new mixture composition and temperature variation.

It is clear that the study of seafloor hydrothermal systems creates more critical questions which remain to be answered. The details of connection between the subsurface magma heat supply and ridge axis hydrothermal venting activity are far from clear. All of these issues need to be studied in further research.

REFERENCES

Anderson, R.N and J.N. Skilbeck (1981), Oceanic heat flow, in *The Sea*, *7*, *The Oceanic Lithoshphere*, ed. by C. Emiliani, 489-523, Wiley-Interscience, New York.

Baker, E.T. (1994), A six-year time series of hydrothermal plumes over the Cleft segment of the Juan de Fuca Ridge, *J. Geophys. Res.*, *99*, 4889-4904.

Baker, E.T. and C.R. German (2004), On the global distribution of hydrothermal vent fields, in *Mid-Ocean Ridges*: *Hydrothermal Interactions Between the Lithosphere and Oceans*, *Geophys. Monogr., 148*, ed. by C.R. German, J. Lin and L.M. Parson, pp. 245-266, Amer. Geophys. Union, Washington, D.C.

Baker, E.T., C.R. German, and H. Elderfield (1995), Hydrothermal plumes over spreading center axes: Global distributions and geological inferences. In *Seafloor Hydrothermal Systems*: *Physical, Chemical, Biological and Geological Interactions*, *Geophys. Monogr.*, *91*, ed. by S.E. Humphris, R.A. Zierenberg, L.S. Mullineaux, and R.E. Thomson, pp. 47-71, Amer. Geophys. Union, Washington, D.C.

Baker, E.T. and G.J. Massoth (1986), Hydrothermal plume measurements: A regional perspective, *Science*, *234*, 980-982.

Baker, E.T. and G.J. Massoth (1987), Characteristics of hydrothermal plumes form two vent fields on the Juan de Fuca Ridge, northeast Pacific Ocean, *Earth Planet. Sci. Lett.*, *85*, 59-73.

Baker, E.T., G.J. Massoth, S.L. Walker, and R.W. Embley (1993), A method for quantitatively estimating diffuse and discrete hydrothermal discharge, *Earth Planet. Sci. Lett.*, *118*, 235-249.

Brandeis G. and C. Jaupart (1986), On the interaction between convection and crystallization in cooling magma chambers, *Earth Planet. Sci. Lett.*, *77*, 345-361.

Becker, K., R. Von Herzen, J. Kirklin, R. Evans, D. Kadko, M. Kinoshita, O.

Matsubayashi, R. Mills, A. Schultz, and P. Rona (1996), Conductive heat flow at the TAG active hydrothermal mound: Results from 1993-1995 submersible surveys, *Geophys., Res. Lett.*, *23*, 3463-3466.

Bergantz, G.W. (2000), On the dynamics of magma mixing by reintrusion: Implications for pluton assembly processes, *J. Struct. Geol.*, *22*, 1297–1309.

Bodvarsson, G. (1950), Geophysical methods in prospecting for hot water in Iceland (translated from Danish), *Timarit Verkfraed Islands*., *35*, 49-59.

Bodvarsson, G. (1961), Physical characteristics of natural heat resources in Iceland, Proc. Conf. *New Sources Energy*, *2*, 82-89.

Bodvarsson, G. and R.P. Lowell (1972), Ocean-floor heat flow and the circulation of interstitial waters, *J. Geophys. Res.*, *77*, 4472-4475.

Brikowski, T. and D. Norton (1989), Influence of magma chamber geometry on hydrothermal activity at mid-ocean ridges, *Earth Planet. Sci. Lett.*, *93*, 241-155.

Calvert, A.J. (1995), Seismic evidence for a magma chamber beneath the slow-spreading Mid-Atlantic Ridge, *Nature*, *377*, 410-414.

Canales, J.P, R.S. Detrick, S.M. Carbotte, G.M. Kent, J.B. Diebold, A. Harding, J. Babcock, M.R. Nedimovic, and E. Van Ark (2005), Upper crustal structure and axial topography at intermediate spreading ridges: Seismic constraints from the southern Juan de Fuca Ridge, *J. Geophys., Res.*, *110*, B12104.

Canales, J.P., S.C. Singh, R.S. Detrick, S.M. Carbotte, A. Harding, G.M. Kent, J.B. Diebold, J. Babcock, and M.R. Nedimovic (2006), Seismic evidence for variations in axial magma chamber properties along the southern Juan de Fuca Ridge, *Earth. Planet. Sci. Lett.*, *246*, 353-366.

Campbell, A.C., T.S. Bowers, C.I. Measures, K.K. Falkner, M. Khadem, and J.M. Edmond (1988a), A time series of vent fluid compositions from 21°N, East Pacific Rise (1979,1981,1985), and the Guaymas Basin, Gulf of California (1982,1985), *J.*

Geophys. Res., *93*, 4537-4549.

Cann, J.R., M.R.Strens, and A.Rice (1985), A simple magma-driven thermal balance model for the formation of volcanogenic massive sulphides, *Earth Planet. Sci. Lett.*, *76*, 123-134.

Collier, J.S. and M.C. Sinha (1990), Seismic images of a magma chamber beneath the Lau Basin back-arc spreading centre, *Nature*, *346*, 646-648.

Collier, J.S. and M.C. Sinha (1992), Seismic mapping of a magma chamber beneath the Valu Fa Ridge, Lau Basin, *J. Geophys. Res.*, *97*, 14031-14053.

Converse, D.R., H.D. Holland, and J.M. Edmond (1984), Flow rates in the axial hot springs of the East Pacific Rise (21°N): Implications for the heat budget and the formation of massive sulfide deposits, *Earth Planet. Sci. Lett.*, *69*, 159-175.

Corliss, J.B., J. Dymond, L.I. Gordon, J.M. Edmond, R.P.Von Herzen, R.D. Ballard, K. Green, D. Williams, A. Bainbridge, K. Crane, and T.H. Van Andel. (1979), Submarine thermal springs on the Galapagos Rift, *Science*, *203*, 1073-1083.

Detrick, R.S., P. Buhl, E. Vera, J. Mutter, J. Orcutt, J. Madsen, and T. Brocher (1987), Multi-channel seismic imaging of a crustal magma chamber along the East Pacific Rise, *Nature*, *326*, 35-41.

Detrick, R.S., A.J. Harding, G.M. Kent, J.A. Orcutt, J.C. Mutter, and P. Buhl (1993), Seismic structure of the southern East Pacific Rise, *Science*, *259*, 499-503.

Edmond, J.M., C. Measures, R.E. McDuff, L.H. Chan, R. Collier, B. Grant, L.I. Gordon, and J.B. Corliss (1979), Ridge crest hydrothermal activity and the balances of the major and minor elements in the ocean: The Galapagos data, *Earth Planet. Sci. Lett.*, *46*, 1-18.

Embley, R.W, W.W. Chadwick, Jr., I.R. Jonasson, D.A. Butterfield, and E.T. Baker (1995), Initial results of the rapid response to the 1993 CoAxial event: relationships between hydrothermal and volcanic process, *Geophys. Res. Lett.*, *22*, 143-146.

Fehn, U., K.E. Green, R.P. Von Herzen, and L.M. Cathles (1983), Numerical models for the hydrothermal field at the Galapagos spreading center, *J. Geophys. Res.*, *88*, 1033-1048.

Fisher, A.T. and K. Becker (1995), Correlation between seafloor and basement relief: Observational constraints and numerical examples and implications for upper crustal permeability, *J. Geophys. Res.*, *100*, 12641-12657.

Fisher, A.T., K. Becker, T.N. Narasimhan, M.G. Langseth and M.J. Mottl (1990), Passive, off-axis convection through the southern flank of the Costa Rica rift, *J. Geophys. Res.*, *95*, 9343-9370.

Fouquet, Y., U. Von Stackelberg, J.L. Charlou, J.P. Donval, J. Erzinger, J.P. Foucher, P. Herzig, R.K. Muehe, S. Soakai, M. Wiedicke, and H. Whitechurch (1991), Hydrothermal activity and metallogenesis in the Lau back-arc basin, *Nature*, *349*, 778-781.

Fouquet, Y., U. Von Stackelberg, J.L. Charlou, J. Erzinger, P.M. Herzig, R. Muehe, and M. Wiedicke (1993), Mettallogenesis in back-arc environments: The Lau Basin example, *Econ. Geol.*, *88*, 2154-2181.

Fretzdorff, S., U. Schwarz-Schampera, H.L. Gibson, C.D. Garbe-Schönberg, F. Hauff, and P. Stoffers (2006), Hydrothermal activity and magma genesis along a propagating back-arc basin: Valu Fa Ridge (southern Lau Basin), *J. Geophys. Res.*, *111*, B08205.

Gendron, J.F., J.F. Todd, R.A. Feely, E.T. Baker, and D. Kadko (1994), Excess ^{222}Rn over the Cleft segment, Juan de Fuca Ridge, *J. Geophys. Res.*, *99*, 5007-5015.

Gente, P., J.M. Auzende, V. Renard, Y. Fouquet, and D. Bideau (1986), Detailed geological mapping by submersible of the East Pacific Rise axial graben near 13°N, *Earth Planet. Sci. Lett.*, *78*, 224-236.

Ginster, U., M.J. Mottl, and R.P. Von Herzen (1994), Heat flux from black smokers on the Endeavor and Cleft segments, Juan de Fuca Ridge, *J. Geophys. Res., 99,* 4937-4950.

Green, K.E., R.P. Von Herzen, and D.L. Williams (1981), The Galapagos Spreading Center at 86W: A detailed geothermal field study, *J. Geophys. Res.*, *86*, 979-986.

Haymon, R.M (1996), The response of ridge-crest hydrothermal systems to segmented, episodic magma supply, *Geological Society Special Publication*, *118*, 157-168.

Haymon, R.M., D.J. Fornari, K.L. Von Damm, M.D. Liley, M.R. Perfit, J. M. Edmond, W. C. Shanks, III, R. A. Lutz, J. M. Grebmeier, S. Carbotte, D. Wright, E. McLaughlin, M. Smith, N. Beedle, and E. Olson (1993), Volcanic eruption of the mid-ocean ridge along the east Pacific Rise crest at 9°45′- 52′N: direct submersible observations of seafloor phenomena associated with an eruption event in April, 1991. *Earth Planet. Sci. Lett.*, *119*, 85–101.

Haymon, R.M., D.J. Fornari, M.H. Edwards, S. Carbotte, D. Wright, and K.C. Macdonald (1991), Hydrothermal vent distribution along the East Pacific Rise crest (9°09′-54′N) and its relationship to magmatic and tectonic processes on fast-spreading mid-ocean ridges. *Earth Planet. Sci. Lett.*, *104*, 513-534.

Hort, M. (1997), Cooling and crystallization in sheet-like magma bodies revisited, *J. Volcanol. Geotherm. Res.*, *76*, 297-317.

Horton, C.W., and F.T. Rogers, Jr., (1945), Convection currents in porous media, *J. Appl. Phys.*, *16*, 367-370.

Humphris, S.E. and J.R. Cann (2000). Constraints on the energy and chemical balances of the modern TAG and ancient Cyprus seafloor sulfide deposits, *J. Geophys. Res.*, *105*, 28477-28488.

Huppert, H.E. and R.S.J. Sparks (1988), The generation of granitic magmas by intrusion of basalt into continental crust, *J. petrology*, *29*, 599-624.

Jannasch, H.W. (1995), Microbial interactions with hydrothermal fluids, in *Seafloor Hydrothermal System*, ed. by S.E. Humphris, R.A. Zierenberg, L.S.Mullineaux and R.E. Thomson, *Geophys. Monogr*., *91*, 273-296, Amer. Geophys. Union, Washington, D.C.

Jarvis, G.T. and W.R. Peltier (1989), Convection models and geophysical observations, in *Mantle Convection*: *Plate Tectonics and Global Dynamics*, ed. W.R. Peltier, Gordon and Breach Science Publishers, 479-595.

Jaupart, C. and S. Tait (1995), Dynamics of differentiation in magma reservoirs, *J. Geophys. Res.*, *100*, 17615-17636.

Jellinek, A.M. and R.C. Kerr (1999), Mixing and compositional stratification produced by natural convection 2. Applications to the differentiation of basaltic and silicic magma chambers and komatiite lava flows, *J. Geophys. Res.*, *104*, 7203-7218.

Jupp, T. and A. Schultz (2000), A thermodynamic explanation for black smoker temperatures, *Nature*, *403*, 880-883.

Kelley, D.S., J.A. Baross, and J.R. Delaney (2002), Volcanoes, fluids, and life at mid-ocean ridge spreading centers, *Annu. Rev. Earth Planet. Sci*., *30*, 385-491.

Kelley, D.S., J.A. Karson, D.K. Blackman, G.L. Frueh-Green, D.A. Butterfield, M.D. Lilley, E.J. Olson, M.O. Schrenk, K.K. Roe, G.T. Lebon, and P. Rivizzigno (2001), An off-axis hydrothermal vent field near the Mid-Atlantic Ridge at 30ºN. *Nature*, 412, 145-149.

Kent, G.M., A.J. Harding, and J.A. Orcutt (1990), Evidence for a smaller magma chamber beneath the East Pacific Rise at 9º30´N, *Nature*, *344*, 650-652.

Lapwood, E. (1948), Convection of a fluid in a porous media, *Proc. Cambridge Philos. Soc.*, *44*, 508-521.

Lejeune, A.M. and P. Richet, (1995), Rheology of crystal-bearing silicate melts: an experimental study at high viscosities, *J. Geophys. Res.*, *100*, 4215-4229.

Lister, C.R.B. (1974), On the penetration of water into hot rock, *Geophys. J. R. Astron. Soc*., *39*, 465-509.

Lister, C.R.B. (1983), The basic physics of water penetration into hot rocks, in *Hydrothermal Processes at Seafloor Spreading Centers*, ed. by P.A. Rona, K. Bostrom, L. Laubier and K.L.Jr. Smith, , 141-168, Plenum, New York.

Lonsdale, P. and K. Becker (1985), Hydrothermal plumes, hot springs, and conductive heat flow in the Southern Trough of Guaymas Basin, *Earth Planet. Sci. Lett.*, *73*, 211-225.

Lowell, R.P. (1975), Circulation in fractures, hot springs, and convective heat transport on mid-ocean ridge crests, *Geophys. J. R. Astron. Soc., 40*, 351-365.

Lowell, R.P. (1980), Topographically driven sub-critical hydrothermal convection in the oceanic crust. *Earth Planet. Sci. Lett.*, *49*, 21-28.

Lowell, R.P. (1991), Modeling continental and submarine hydrothermal systems, *Rev. Geophys.*, *29*, 457-476.

Lowell, R.P. and D.K. Burnell (1991), A numerical model for magma-hydrothermal boundary layer heat transfer in the oceanic crust, *Earth Planet. Sci. Lett.*, *104*, 59-69.

Lowell, R.P., B.W. Crowell, S.R. Gosnell, K.C. Lewis, L. Liu, and Y. Yang (2007a), Modeling multiphase, multi-component processes at oceanic spreading centers: Magma to microbe, in *Modeling hydrothermal processes at Oceanic Spreading Centers*: *Magma to Microbe*, *Geophys. Monogr.*, *XX*, ed. by R.P. Lowell, J.S. Seewald, M.R. Perfit and A. Metaxas, pp. xx, Amer. Geophys. Union, Washingto, D.C. (submitted).

Lowell, R.P. and L.N. Germanovich (1994), On the temporal evolution of high-temperature hydrothermal systems at ocean ridge crests, *J. Geophys. Res.*, *99*, 565-575.

Lowell, R.P. and L.N. Germanovich (1995), Dike injection and the formation of megaplumes at ocean ridges, *Science*, *267*, 1804-1807.

Lowell, R.P. and L.N. Germanovich (2004), Seafloor hydrothermal processes: Results

from scale analysis and single-Pass models, in *Mid-Ocean Ridges*: *Hydrothermal Interactions Between the Lithosphere and Oceans, Geophys. Monogr. Ser.*, *148*, ed. by C.R. German, J. Lin and L.M. Parson, pp.219-244, Amer. Geophys. Union, Washington, D.C.

Lowell, R.P. and P.A. Rona (1985), Hydrothermal models for the generation of massive sulfide ore deposits, *J. Geophys. Res.*, *90*, 8769-8783.

Lowell, R.P., P. A. Rona, and R. P. Von Herzen (1995), Seafloor hydrothermal systems, *J. Geophys. Res.*, *100*, 327-352.

Macdonald, K.C., K. Becker, F.N. Spiess, and R.D. Ballard (1980), Hydrothermal heat flux of the "black smoker" vents on the East Pacific Rise, *Earth Planet. Sci. Lett.*, *48*, 1-7.

Maclennan, J. (2007), The supply of heat to mid-ocean ridges by crystallization and cooling of mantle melts, in *Modeling hydrothermal processes at Oceanic Spreading Centers*: *Magma to Microbe*, *Geophys. Monogr.*, *XX*, ed. by R.P. Lowell, J.S. Seewald, M.R. Perfit and A. Metaxas, pp. xx, Amer. Geophys. Union, Washingto, D.C. (submitted).

MacLeod, C.J. and G. Yaouancq (2000), A fossil melt lens in the Oman ophiolite: Implications for magma chamber processes at fast spreading ridges, *Earth Planet. Sci. Lett.*, *176*, 357-373.

Marsh, B.D. (1981), On the crystallinity, probability of occurrence, and rheology of lava and magma, *Contrib. Mineral. Petrol.*, *78*, 85-98.

Martin, D. (1990), Crystal settling and in situ crystallization in aqueous solutions and magma chambers, *Earth Planet. Sci. Lett.*, *96*, 336-348.

Martin, D. and R. Nokes (1989), A fluid dynamical study of crystal settling in convecting magmas, *J. Petrol.*, *30*, 1471-1500.

McConachy, T.F., R.D. Ballard, M.J. Mottl, and R.P. Von Herzen (1986), Geological form and setting of a hydrothermal vent field at latitude 10°56'N, East Pacific Rise: A detailed study using *Angus* and *Alvin*, *Geology, 14,* 295-298.

Oldenburg, C.M, F.J. Spera, D.A. Yuen, and G.H, Sewell (1989), Dynamic mixing in magma bodies: theory, simulations and implications, *J. Geophys. Res.*, *94*, 9215-9236.

Parsons, B. and J.G. Sclater (1977), An analysis of the variation of ocean floor bathymetry and heat flow with age, *J. Geophys. Res.*, *82*, 803-827.

Rabinowicz, M., J.C. Sempere, and P. Genthon (1999), Thermal convection in a vertical permeable slot: Implications for hydrothermal circulation along mid-ocean ridges*, J. Geophys. Res.*, *104*, 29275-29292.

Ramondenc, P., L.N. Germanovich, K.L. Von Damm, and R.P. Lowell (2006), The first measurements of hydrothermal heat out at 9°50´N, East Pacific Rise, *Earth Planet. Sci. Lett.*, *245*, 487-497.

Ribando, R.J., K.E. Torrance, and D.L. Turcotte (1976), Numerical models for hydrothermal circulation in the oceanic crust, *J. Geophys. Res.*, *81*, 3007-3012.

Rohr, K.B., B. Mildreit and C.J. Yorath (1988), Asymmetric deep crustal structure across the Juan de Fuca Ridge, *Geology*, *16*, 533-537.

Rona, P.A., M.D. Hannington, C.V. Raman, G. Thompson, M.K. Tivey, S.E. Humphris, L. Lalou, and S. Petersen (1993), Active and relict sea-floor hydrothermal mineralization: TAG hydrothermal field, Mid-Atlantic Ridge 26°N, 45°W, *Econ. Geol., 88,* 1989-2017.

Rona, P.A. and D.A. Trivett (1992), Discrete and diffuse heat transfer at ASHES vent field, Axial Volcano, Juan de Fuca Ridge, *Earth Planet. Sci. Lett., 109,* 57-71.

Roscoe, R. (1952), The viscosity of suspensions of rigid spheres. *British Journal of Applied Phys.*, *3*, 267-269.

Rosenberg, N.D., J.E. Lupton, D. Kadko, R. Collier, M.D. Lilley, and H. Pak (1988), Estimation of heat and chemical fluxes from a seafloor hydrothermal vent field using radon measurements, *Nature, 344*, 604-607.

Rudnicki, M.D. and H. Elderfield (1992), Theory applied to the Mid-Atlantic Ridge hydrothermal plumes: the finite difference approach, *J. Volcanol. Geotherm. Res.*, *50*, 161-172.

Rudnicki, M.D. and C.R. German (2002), Temporal variability of the hydrothermal plume above the Kairei vent field, 25°S, Central Indian Ridge, *Geochem. Geophys. Geosyst.*, *3*, 10.1029/2001GC000240.

Schoofs, S. and U. Hansen (2000), Depletion of a brine layer at the base of ridge-crest hydrothermal system, *Earth Planet. Sci. Lett.*, *180*, 341-353.

Schultz, A., J.M. Delaney, and R.E. McDuff (1992), On the partitioning of heat flux between diffuse and point source venting, *J. Geophys. Res., 97,* 12229-12314.

Shank, T.M, D.J. Fornari, K.L. Von Damm, M.D. Lilley, R.M. Haymon, and R.A. Lutz (1998), Temporal and spatial patterns of biological community development at nascent deep-sea hydrothermal vents along the East Pacific Rise, *Deep Sea Res. II*, *45*, 465-515.

Shaw, H.R. (1980), The fracture mechanisms of magma transport from the mantle to the surface. In: *Physics of Magmatic Processes*, ed. by Hargraves, R.B., Princeton University Press, 201-264.

Singh, S.C., J.S. Collier, A.J. Harding, G.M. Kent, and J.A. Orcutt (1999), Seismic evidence for a hydrothermal layer above the solid roof of the axial magma chamber at the southern East Pacific Rise, *Geology*, *27*, 219-222.

Singh, S.C., W.C. Crawford, H. Carton, T. Seher, V. Combier, M. Cannat, J.P. Canales, D. Dusunur, J. Escartin, and J.M. Miranda (2006), Discovery of a magma chamber and faults beneath a Mid-Atlantic Ridge hydrothermal field, *Nature*, *442*, 1029-1032.

Sinha, M.C. (1995), Segmentation and rift propagation at the Valu Fa Ridge, Lau Basin: evidence from gravity data, *J. Geophys. Res.*, *100*, 15025-15043.

Sinha, M.C., S.C. Contable, C. Peirce, A. White, G.S. Heinson, L.M. MacGregor, and D.A. Navin (1998), Magmatic processes at slow spreading ridges: implications of the RAMESSES experiment at 57°45'N on the Mid-Atlantic Ridge, *Geophys. J. Int.*, *135*, 731-745.

Sinton, J.M. and R.S. Detrick (1992), Mid-ocean ridge magma chambers, *J. Geophys. Res.*, *97*, 197-216.

Spera, F.J. (2000), Physical properties of magma, in *Encyclopedia of Volcanoes*, Academic Press, 171-190.

Spiess, F.N., K.C. Macdonald, T. Atwater, R. Ballard, A. Carranza , D.Cordoba, C. Cox, V.M. Diaz Garcia, J. Francheteau, J. Guerrero, J. Hawkins, R. Haymon, R. Hessler, T. Juteau, M. Kastner, R. Larson, B. Luyendyk, J.D. Macdougall, S. Miller, W. Normark, J. Orcutt, and C. Rangin (1980), East Pacific Rise: Hot springs and geophysical experiments, *Science*, *207*, 1421-1433.

Stein, C.A. and S. Stein (1992), A model for the global variation in oceanic depth and heat flow with lithospheric age, *Nature*, *359*, 123-129.

Stein, C.A. and S. Stein (1994), Constraints on hydrothermal heat flux through the oceanic lithosphere from global heat flow, *J. Geophys. Res.*, *99*, 3081-3095.

Stein, J.S. and A.T. Fisher (2001), Multiple scales of hydrothermal circulation in Middle Valley, northern Juan de Fuca Ridge: Physical constraints and geologic models, *J. Geophys. Res.*, *106*, 8563-8580.

Strens, M.R. and J.R. Cann (1982), A model of hydrothermal circulation in fault zones at mid-ocean ridge crests, *Geophys. J. Roy. Astr. Soc.*, *71*, 225-240.

Strens, M.R. and J.R. Cann (1986), A fracture-loop thermal balance model of black smoker circulation, *Tectonophysics*, *122*, 307-324.

Tivey, M.K. and J.R. Delaney (1986), Growth of large sulfide structures on the Endeavour Segment of the Juan de Fuca Ridge, *Earth. Planet. Sci. Lett.*, *77*, 303-317.

Turner, I.M., C. Peirce, and M.C. Sinha (1999), Seismic imaging of the axial region of the Valu Fa Ridge, Lau Basin-the accretionary processes of an intermediate back-arc spreading ridge, *Geophys. J. Int.*, 138, 495-519.

Turner, J.S. (1973), *Buoyancy effects in fluids*, Cambridge University Press, London.

Veirs, S.R., R.E. McDuff, and F.R. Stahr (2006), Magnitude and variance of near-bottom horizontal heat flux at the Main Endeavour hydrothermal vent field, *Geochem. Geophys. Geosyst.*, *7*, Q02004, doi:10.1029/2005GC000952.

Von Damm, K.L. (2001), Lost City found. *Nature*, *412*, 127-128.

Von Damm, K.L., S.E. Oosting, R. Kozlowski, L.G. Buttermore, D.C. Colodner, H.N. Edmonds, J.M. Edmond, and J.M. Grebmeier (1995), Evolution of East Pacific Rise hydrothermal vent fluids following a volcanic eruption, *Nature*, *375*, 47-50.

Von Damm, K.L., C.M. Parker, R.M. Gallant, and J.P. Loveless (2002), Chemical evolution of hydrothermal fluids from EPR 21°N: 23 years later in a phase separating world, *EOS Trans*., Amer. Geophys. Union, *83*, Suppl., 1421.

Wilcock, W.S.D. (1998), Cellular convection models of mid-ocean ridge hydrothermal circulation and the temperatures of black smoker fields, *J. Geophys. Res.*, *103*, 2585-2596.

Wilcock, W.S.D. and J.R. Delaney (1996), Mid-ocean ridge sulfide deposits: Evidence for heat extraction from magma chambers or cracking fronts?, *Earth Planet. Sci. Lett.*, *145*, 49-64.

Williams, D.L. and R.P. Von Herzen (1974), Heat loss from the Earth: New estimate, *Geology*, *2*, 327-328.

Williams, D.L., R.P. Von Herzen, J.G. Sclater, and R.N. Anderson (1974), The Galapagos Spreading Center: lithospheric cooling and hydrothermal circulation, *Geophys. J. Roy. Astr. Soc.*, *38*, 587-608.

Worster, M.G., H.E. Huppert, and R.S.J. Sparks (1990), Convection and crystallization in magma cooled from above, *Earth Planet. Sci. Lett.*, *101*, 78-89.

Wright, D.J., R.M. Haymon, and D.J. Fornari (1995), Crustal fissuring and its relationship to magmatic and hydrothermal processes on the East Pacific Rise crest 9°12′ to 54′N, *J. Geophys. Res., 100*, 6097-6120.